VARIABILITY AND CONTROL OF ACTIVITY IN SMALL NEURAL NETWORKS: EFFECTS OF NEURON FEEDBACK DYNAMICS

A Dissertation
Presented to
The Academic Faculty

by

Ryan Hooper

In Partial Fulfillment
of the Requirements for the Degree
Doctor of Philosophy in the
School of Biomedical Engineering

Georgia Institute of Technology
May, 2016

VARIABILITY AND CONTROL OF ACTIVITY IN SMALL NEURAL NETWORKS: EFFECTS OF NEURON FEEDBACK DYNAMICS

Approved by:

Dr. Astrid Prinz, Advisor
Department of Biology
Emory University

Dr. Gennady Cymbalyuk
Neuroscience Institute
Georgia State University

Dr. Robert Butera
School of Biomedical Engineering
School of Electrical and Computer Engineering
Georgia Institute of Technology

Dr. Dieter Jaeger
Department of Biology
Emory University

Dr. Carmen Canavier
Department of Cell Biology and Anatomy
Neuroscience Center of Excellence
Lousiana State University Health Sciences Center

Date Approved: [January 04, 2016]

ACKNOWLEDGEMENTS

First, I want to thank those who made significant contributions to the intellectual content of this work: Astrid, Carmen, Ruben, and Gennady, thank you so much for your time, insights, brainstorming with me. Learning from each of you has enriched how I think and approach scientific questions.

To my committee, thank you for your time, efforts, and steady guidance. I am indebted to each of you.

To the Prinz lab: Tomasz for the half-caff and continually sparking our imagination of neurons and computation; Fred for being the trailblazer, investing in me, and being Fred; Wafa for always being available to bounce ideas off of each other and generally being amazing to work with; Cengiz for the puns and mentoring; Amber, Santiago, Andrei, Kun, and everyone else: thank you.

To other professionals: Selva and Wulf-Dieter for all the conversations. To Doug and everyone at Takeda, thank you for the encouragement and support.

To my family, my friends, Canary, Paul. Thank you!

TABLE OF CONTENTS

LIST OF FIGURES

SUMMARY

Rhythmic neural networks are dynamic systems that reliably generate stereotyped activity that drives numerous biological processes essential to life, including motor pattern generation. Due to these networks' reliable pattern generation, as well as the broad wealth of insights into fundamental questions in neuroscience that have been gained in their study without considering their fundamentally stochastic nature, the variability in their pattern generation is often overlooked. But such rhythmic networks are typically composed of a richly diverse ensemble of neurons, synapses, and their underlying properties and kinetics, each of which possesses individual dynamics that interact to contribute to the collective network dynamics that determine not just steady-state neural network activity, but also the presence or absence of network reliability and stability in the face of perturbations and stochastic processes. Because the crustacean stomatogastric network is a well studied and understood network, is experimentally amenable, and has been modeled extensively, it serves as a good system for investigating the role specific features of network composition play in determining network activity variability. Advances here may readily be adapted to inform models that are currently the focus of intense study aimed at gaining an understanding of the connection between underlying molecular and genetic cell properties and rhythmic neural network activity.

The primary focus of this research is to explore the impacts of one such feature of network composition that is involved in stochastic network activity—the dynamics of synaptic feedback—and in turn determining its impact on variability of the pacemaker network. We have discovered that synaptic feedback dynamics in the crustacean

stomatogastric pattern generating network tend to be ordered in multiple senses that optimally minimize rhythmic variability: in terms of both feedback neuron phase response properties, and cycle-by-cycle phase maintenance of synaptic feedback burst width. Our findings have implications for neural network design and optimization as well as neural network model and database construction.

CHAPTER 1: INTRODUCTION

INTRODUCTION

Neural networks and oscillations

Networks of neurons connected to one another form the patterned activity that generates the higher functions underlying life. In particular, neural networks are central to many important rhythmic nervous system functions including motor and behavioral tasks such as walking (Llinás, 1988; Ramirez et al., 2004), the coordination of breathing (Koshiya and Smith, 1999), and memory and cognition (Buzsáki et al., 1994; Engel et al., 2001). Such rhythmic neural networks characteristically involve oscillations (Berger, 1929; Buzsáki, 2004). Many debilitating neural disorders have been found to be associated with dysfunction in the rhythmogenesis of these oscillations, including epilepsy (Worrell et al., 2004; Zijlmans et al., 2012), Parkinson's Disease (Brown et al., 2001), and schizophrenia (Spencer et al., 2003; Uhlhaas et al., 2008). So there has been much study of how networks give rise to oscillations and what is the nature of those oscillations in order to better understand disease (Yu et al., 2008; Rieubland et al., 2014).

Invertebrate nervous systems also display rhythmic oscillations (Selverston, 2010), and are amenable to studying the relationship between networks and their associated oscillatory activity due to their small network structure. In this work we will utilize these networks to examine the relationships between rhythmic networks and variability in their oscillatory activity.

Rhythmic networks and coupled oscillators

Rhythmic neural networks are networks characterized by oscillatory activity with repeating intervals of high membrane voltage alternating with intervals of low membrane voltage. In many well studied networks, rhythmic activity takes the form of depolarized intervals with multiple successive action potentials supported by plateau potentials (a burst), interspersed with quiescent hyperpolarized intervals (Russell and Hartline, 1978; Miller and Selverston, 1982). Spontaneous rhythmic activity can be generated by a neuron endogenously, arising purely from the nonlinear activation and inactivation dynamics of the neuron's membrane properties.

Neurons in network capable of endogenous oscillatory activity that exert influence on one another via synaptic connections are said to be coupled oscillators (Glass, 2001; Winfree, 2001; Ermentrout and Chow, 2002). Here it is helpful to define activity intervals in each neuron in such a coupled oscillator (Figure 1): for two-neuron networks, the time interval between the beginning of one neuron's cycle period (initiated with a spike or burst) and the time when it receives synaptic input from another neuron in the network is referred to as the stimulus interval (ts). Next, the time between the receipt of a synaptic input and the initiation of the next burst (ending the cycle period) is referred to as the response interval (tr).

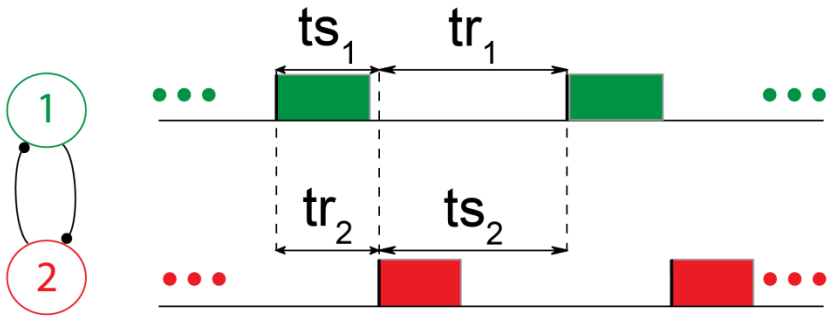

Figure 1. Firing intervals for two coupled neurons. ts_1: stimulus interval for the first neuron; tr_1: response interval for the second neuron. ts_2: stimulus interval for the second neuron; tr_2: response interval for the second neuron. Note that the stimulus interval of one neuron is equal to the response interval of its partner.

Phase response analysis and the t_S-t_R curve

One powerful extension of pulse coupled oscillator theory, called phase response analysis, has been used to study how network dynamics arise from interactions between the neurons comprising the network. In phase response analysis, a neuron's output (spike or burst) occurring at the interval tr that occurs in response to an immediately preceding input given at a certain stimulus interval ts is tabulated for many intervals ts (Fig. 2A), giving us a phase resetting curve (PRC) (Fig. 2B). The study of PRCs has proven invaluable to understanding how network activity is generated and how neurons synchronize.

In phase response analysis it is common to compute the single-pulse PRC (spPRC) for pulse-coupled systems (Fig. 2A), which means that a single pulse is delivered and the response of subsequent cycles P_2, P_3, etc. are not stimulated but observed to measure second and third order resetting, respectively. The spPRC gives us an estimate of how a neuron will respond to a given synaptic input received at different cycle phases. Its measurement is accomplished by perturbing an ongoing oscillatory

rhythm with intrinsic period P_{Int} at phase $\varphi = t_S/P_{Int}$ with a stimulus that begins at stimulus delay *ts*, and tabulating the resulting normalized changes in network period. This results in the first order PRC, $f_1(\varphi) = (P_1 - P_{Int})/P_{Int}$, the second order PRC $f_2(\varphi) = (P_2 - P_{int})/P_{int}$, and so on ($f_1$ is illustrated in Fig. 2B).

A multiple-pulse PRC (mpPRC), however, can be measured differently than the spPRC, such that phasic stimulation is applied to each successive cycle (figure 2C). This mpPRC can then be applied to neurons that are not endogenous oscillators (Sieling et al., 2012). Here a perturbation is repeatedly applied at a fixed stimulus interval *ts*, the resultant response interval *tr* is tabulated, then ts is incremented to sample another *tr-ts* relationship. This process is repeated until the entire *tr-ts* region of interest is estimated. The resulting *tr-ts* curve can be utilized as-is as its own variant of the PRC, or used to calculate a normalized phase-based mpPRC in a similar manner to the spPRC, as done for the functional PRC, a type of mpPRC (Cui et al., 2009).

For our purposes we retain the *tr-ts* form because we examine neurons that do not have an intrinsic period of oscillation P_{int}, so phase φ is difficult to define. Therefore for simplicity and consistency we represent all mpPRCs in their *tr-ts* form, even for intrinsically oscillatory neurons.

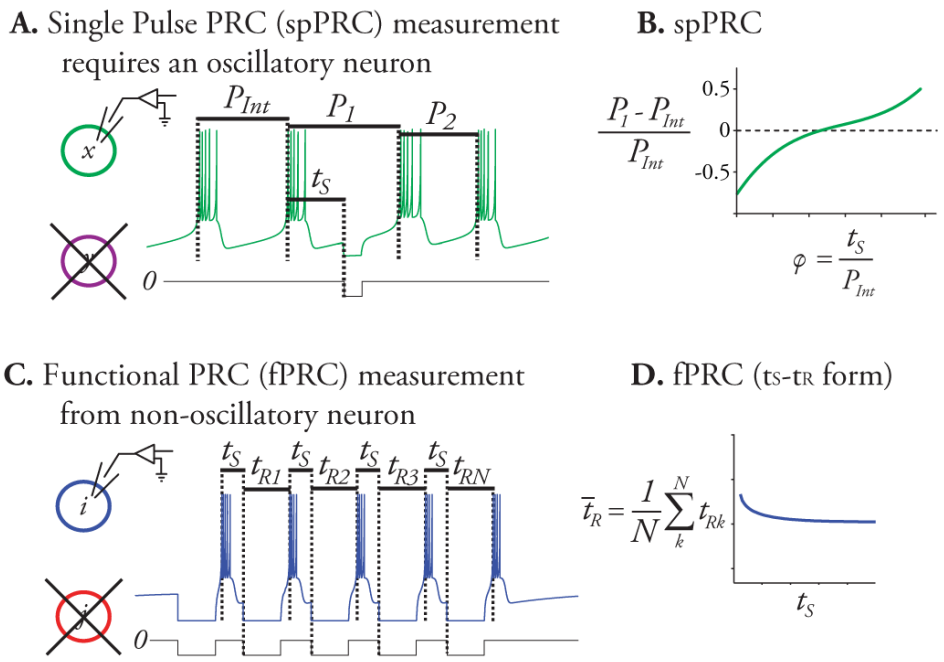

Figure 2. Comparison of single pulse phase response curve (spPRC) and multiple-pulse PRC (mpPRC) analysis. Both measures allow us to characterize how sensitive a neuron is to changes in the onset stimulus interval t_S of synaptic input, but the mpPRC method has the added capability of providing this measure for neurons that are adaptive (Cui et al. 2009) and not intrinsically oscillatory (Sieling et al. 2012). (A) a measurement of the spPRC proceeds by isolating the measured neuron from its synaptic input, then introducing a conductance pulse at stimulus delay t_S from the beginning of the cycle with the dynamic clamp with magnitude and duration designed to approximate a synaptic input. The period of the cycle in which this synaptic input is applied (P_1) is tabulated, as are the following cycles P_2, P_3, etc. (which do not receive a stimulus), and (B) the resulting spPRC is calculated by repeating this process for numerous values of *ts* to sample $0<\varphi<1$. Note here that spPRC values greater than zero indicate a phase delay in the occurance of the beginning of the next burst cycle, while those less than zero indicate a phase advance. (C) calculating the mpPRC is similar, but stimuli are repeated for each cycle with the stimulus delay *ts*. After a number of repeats, when a steady state *tr** is reached, *ts* is incremented to a new value, and this is repeated until (D) the mpPRC curve is constructed. Here the mpPRC is left in the *tr-ts* form, but it can sometimes be calculated in the same normalized form that the spPRC uses (see text), just as the spPRC can be computed in the *tr-ts* form. Figure adapted from Sieling et al. 2012.

The role of variability in rhythm generating neuronal networks

Many networks underlying rhythmic burst generation are thought to convey information by their activity in different ways (Izhikevich et al., 2003). For example, in invertebrates it is believed that spike number in a burst, which correlates with burst width

as we measure it, controls muscle contraction amplitude (Morris and Hooper, 1997). Sometimes even the variability of a rhythmic network can be thought of as a form of information in itself, as when the stick insect *Carausius morosus* uses variability in its walking patterns to evade the visual attention of predators (Hooper et al., 2006; Gabriel and Büschges, 2007), or when the mollusk *Aplysia* attempts different stochastic feeding patterns in order to find an acceptable feeding strategy for consuming food of diverse texture, size, and composition (Horn et al., 2004; Sieling et al., 2014).

If information is conveyed by bursting networks in terms of variation in rhythmic activity, then a natural question that arises asks if real bursting networks possess properties or configurations that support or otherwise control this variation.

Recent research has identified one feature of network structure that is important to invertebrate bursting rhythmic network activity variability, specifically that the variability of burst period of oscillatory neurons can be stabilized by the presence of inhibitory synaptic feedback from a LP follower neuron (Mamiya and Nadim, 2004; Nadim et al., 2011). In such networks, it was shown that variability in cycle period is reduced compared to that observed in the bursting pacemaker when isolated from its synaptic feedback, and that the effect of extrinsic perturbations applied to the pacemaker is reduced. But it should be noted that in each of these experiments the follower neuron element of the network was either composed of a biological neuron or a very simple model with fixed timing. Specific details of how the pyloric network's synaptic feedback influence the effect of reducing variability —including phase response timing and burst width timing—have yet to be explored, and will be in this work.

Further, despite extensive evidence that the timing and variation of bursts are important, such information is generally not considered in mathematical and computational modeling studies of bursting neurons and neuronal networks. In part, a goal of this work is to establish if there are consequences for such simplification in model construction and identify distinctive properties of networks that such simplified models may fail to capture.

The pyloric network

The pyloric network of the crustacean stomatogastric nervous system is a neuronal network of the STG that functions within the larger stomatogastric nervous system (STNS) of crustacea (Fig. 3A) and serves to elicit rhythmic contractions in the muscles of the foregut's pylorus, a process which is involved in food filtration and digestion (Marder and Bucher, 2001). This network's activity consists of a stereotyped triphasic bursting pattern driven by the anterior burster/pyloric dilator (AB/PD) pacemaker complex (Russell and Hartline, 1978; Bal et al., 1988; Harris-Warrick and Marder, 1991), which itself consists of an electrically coupled group of one AB neuron and two PD neurons, all of which burst in synchrony and produce the first phase of the rhythm (Fig. 3B,C,D in green). The AB/PD projects inhibitory synapses to two follower neuron groups within the pyloric network (fig. 3C, synapses with open circles are cholinergic, synapses with filled circles are glutamatergic). The target neurons of these projections are the lateral pyloric neuron (LP, one per STG) and the pyloric neurons (PY, 5-6 each per STG), which are typically each represented as one lumped neuron each in modeling studies due to the strong electrical coupling between PY neurons. Functionally these follower neurons are distinguished by their participation in bursting network

oscillation via post-inhibitory rebound, meaning that they fire bursts following to the application and removal of inhibitory synaptic input. In this way these neurons are conditional bursters at the pyloric network's oscillation frequency, and absent synaptic inhibition are either silent or spike tonically (Fig. 3D).

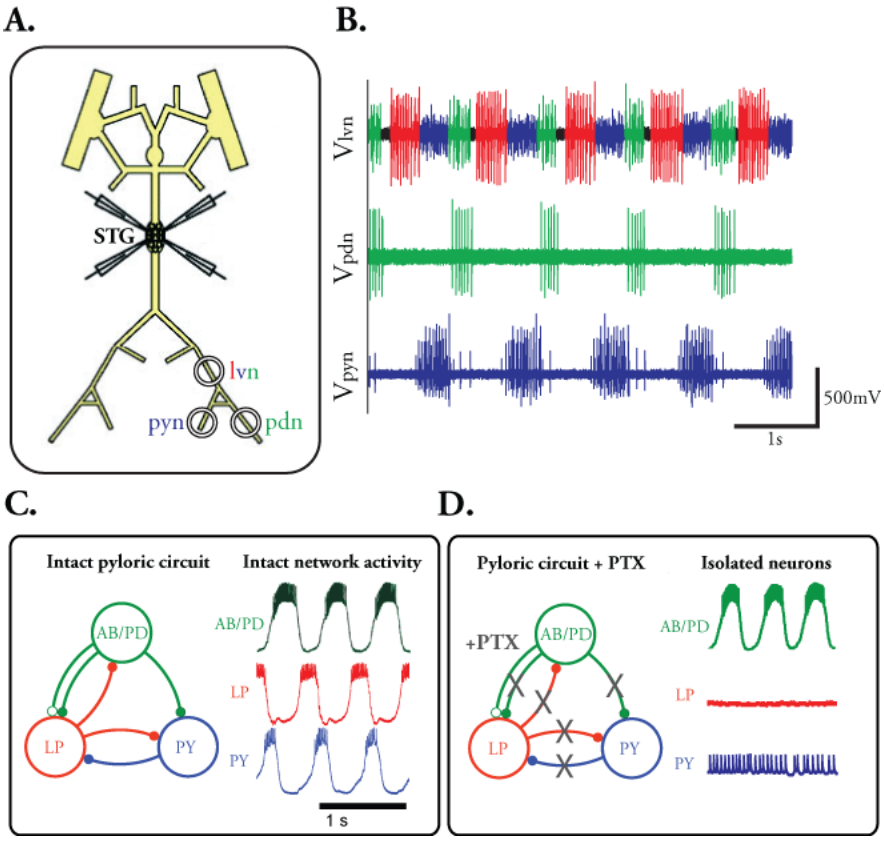

Figure 3. Crustacean stomatogastric nervous system (STNS). (A) The Stomatogastric Ganglion (STG) is amenable to intracellular manipulation via its somata, while extracellular recordings can be measured from the motor nerves: lateroventricular nerve (*lvn*, contains motor nerves for LP [red], PY [blue], and PD[green]), and the nerves of PY and PD (*pyn* and *pdn*). Adapted from Marder and Bucher, 2007. (B) Recorded extracellular traces displaying triphasic rhythm on *lvn*. The intact network pyloric network (C) generates a triphasic bursting rhythm by utilizing a pacemaker neuron group (AB/PD), which leads the rhythm, and two types of follower neurons (LP and PY) that burst in response to post-inhibitory rebound imposed by synaptic input from AB/PD. Reciprocal inhibition between LP and PY and synaptic feedback from LP to PY are important features of this circuit. Bath application of PTX (D) pharmacologically blocks glutamatergic synapses in the pyloric network, which has the effect of synaptically isolating AB/PD, and minimizing synaptic inhibition of the follower neurons. The resulting network activity reveals the intrinsic rhythmicity of AB/PD along with the lack of propensity of LP or PY to burst on their own on a pyloric timescale.

Despite the apparent complexity of this system in generating its stereotyped triphasic rhythmic activity, we do stress that this system is both simple in terms of neuronal central pattern generator circuits and well understood in its composition and connectivity, which together with its experimental tractability and history of study by computational and mathematical modeling, makes it well suited to study the effects of synaptic feedback on oscillations in neuronal networks. Further, bath application of picrotoxin (PTX) to the pyloric network has the effect of blocking all inhibitory glutamatergic synapses in the system, which functionally isolates the AB/PD from synaptic feedback (Fig. 3D), facilitating the construction of hybrid networks using the dynamic clamp (Prinz et al., 2004a).

Variability in the pyloric network

The pacemaker neuron (AB/PD) exhibits variability in both period (P_i) and burst width (B_i), both when receiving feedback inhibition from the follower neurons (Fig. 4, left), and when isolated from the network (Fig. 4, right). Since these features of network activity are important, we will primarily concern ourselves with these measures in our studies. To quantify variability of these measures we will primarily use the standard deviation σ instead of alternative measures of variability such as the coefficient of variation ($CV=\sigma/\mu$), since measures based on a ratio are not appropriate for use in analysis of variance (ANOVA) statistical tests (Sokal and Rohlf, 1995). We make one exception in using the CV during a preliminary study for purposes of consistency with other studies, in which we do not use ANOVA.

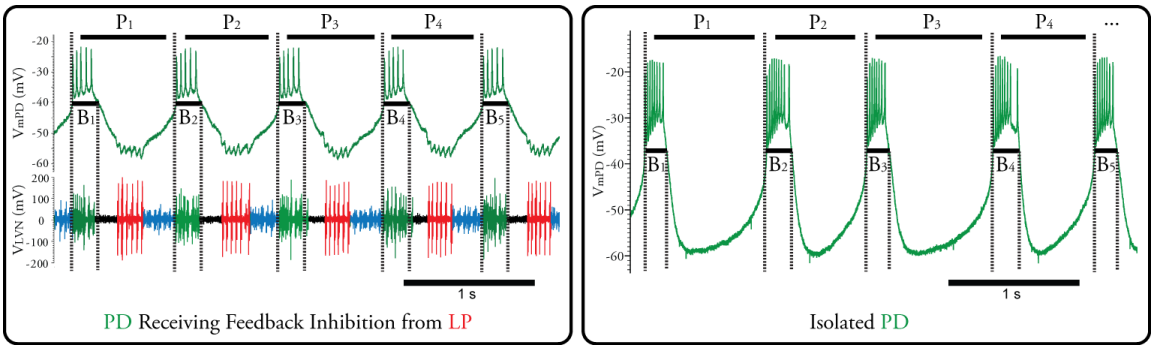

Figure 4. Measures of activity variability in the pyloric network of the STNS, in both the intact network where the pacemaking AB/PD receives inhibitory synaptic feedback from LP (left panel), or when the AB/PD neuron is isolated from synaptic input by application of PTX (right panel). We measure both cycle period (Pi) and burst width (Bi) in the same neuron (AB/PD) in both cases. Intracellular recordings of AB/PD activity are made with sharp electrode recording from PD (V_{mPD}). Extracellular recordings were made from the lvn (V_{lvn}, left). Color coding of the intact network activity matches that of figure 3: AB/PD (green), LP (red), PY (blue).

Hybrid networks

The use of hybrid networks to explore small neuronal networks is a particular development that arose from advances in the dynamic clamp (Prinz et al. 2004), which is the utilization of circuitry or a computer to solve equations that simulate artificial conductances that work to modify the conductance experienced by a biological neuron. The conductances that the dynamic clamp simulates are called artificial because—unlike the biological conductances that exist in a biological neuron, which arise from ion channels embedded in the neuron's plasma membrane and may have disparate effects on the neuron's electrical activity depending upon their spatial distribution and density across the neuron's complex morphology—the dynamic clamp simulates all conductance operations outside of the neuron and typically imposes that conductance on the biological cell in a way that differs from the biological conductance. Dynamic clamp exploits Ohm's law, $I=G \cdot V$, where I is the electrical current, G is the conductance, and V is the membrane potential. When the experimenter using dynamic clamp desires to add or

subtract a given *G* from a neuron, all that is required is to solve for a mathematical model of that G, multiply by the measured membrane voltage *V*, and inject the resulting product into the neuron as a current *I* using standard electrophysiological equipment.

Hybrid networks typically use the dynamic clamp to establish conductance models for artificial synapses, artificial ion channels within biological neurons, and sometimes entire model neurons.

Using the dynamic clamp, we consider hybrid networks which use model neurons that are not modeled based upon the dynamics of the ion channels of the neuron to be modeled as in the popular Hodgkin-Huxley models, but instead utilize the fPRC itself to provide model neuron activity. Because the fPRC contains all necessary information to determine the timing of an neuron's output (at tr) given the timing of the last received input (t_S), all that is required to generate activity identical to that of the neuron the fPRC represents is a way to calculate the activity waveform characteristic of a response to an input, assuming that the input does not vary in duration and strength (Oprisan and Canavier 2005). In such a way, the dynamic clamp is able to map the input of one cycle of the pulse coupled system to the next. Because this only serves to model the output of a neuron and does not directly utilize a neuron's underlying biophysics and electrical dynamics, we refer to it simply as a virtual feedback unit (VFU).

PRELIMINARY STUDIES

Synaptic feedback in a hybrid network reduces activity variability

Previous studies have shown that the presence of inhibitory synaptic feedback is sufficient to significantly reduce variability in period of the AB/PD neuron in both biological preparations and model studies (Nadim et al., 2011). However, it was not immediately clear that we could observe the same effect in a hybrid network constructed with a biological AB/PD and dynamic clamp implemented VFU, due to uncertainties about space clamp limitations, limitations of the maximal conductance that the dynamic clamp can handle (Preyer and Butera, 2009; Hooper and Prinz, 2011), and simplifications that are commonly made to the conductance waveform in dynamic clamp. Nadim et al. did impose artificial synaptic inhibition on an AB/PD using dynamic clamp, but there was no feedback to the PIR neuron to make a true hybrid network, the change in CV was not reported for these experiments, and the synaptic conductance utilized was well above the biological range observed *in vitro* of ~20-90nS (Prinz et al., 2003b; Archila, 2013). So prior to further analysis we tested for period CV reduction from synaptic feedback with our hybrid network in N=7 preparations. The VFU to PD synaptic conductance was set in the middle of the biological range (50nS), and VFU burst timing and duration mimicked that of the biological LP measured in the intact network prior to synaptic blockade with PTX. We observed a highly significant reduction in CV over the isolated AB/PD as measured by a two-tailed paired-samples Student's t-test with $p < 0.001$ (Fig. 5), which are similar to the results obtained in Nadim et al. 2011 for their fully biological preparations.

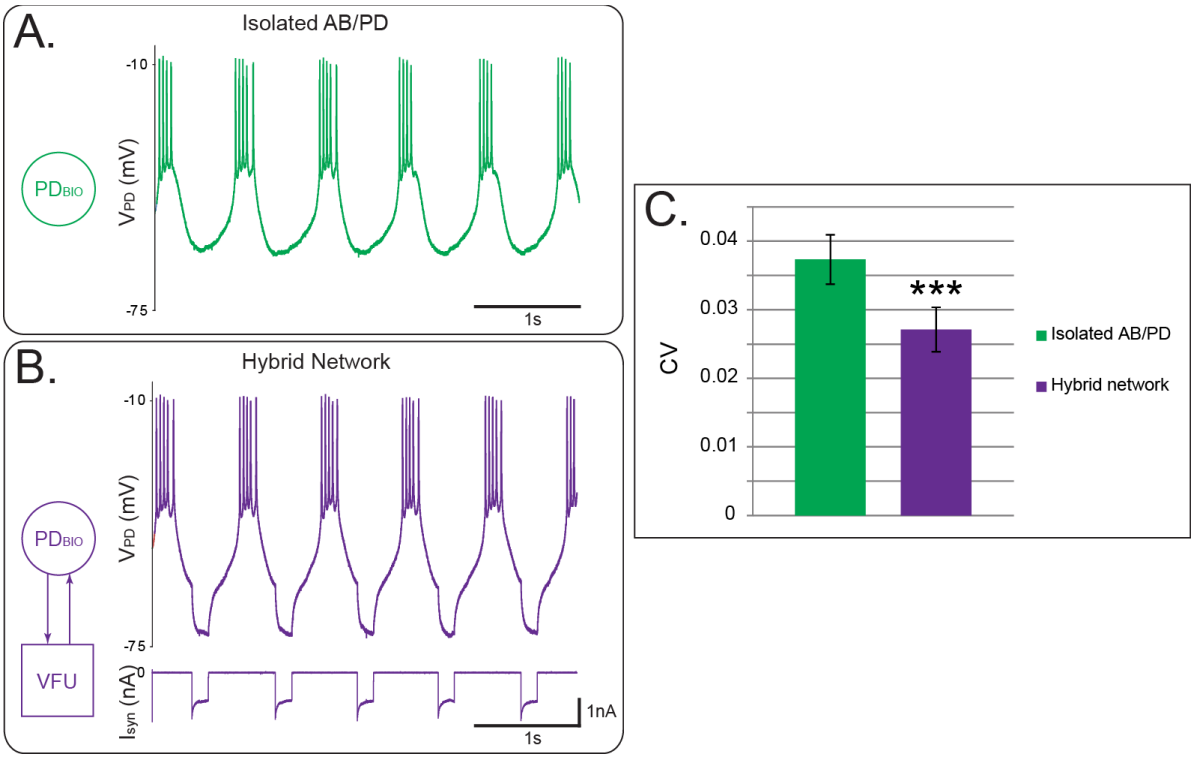

Figure 5. Coefficient of Variation (CV) of oscillation period of an isolated AB/PD (A, diagram) compared to a hybrid network (B, diagram) of the same isolated AB/PD with the artificial addition of a VFU introduced using dynamic clamp with LP inspired tr-ts curve and burst duration and synaptic conductance of 50nS. Activity from an example experiment is shown for both the isolated AB/PD (A) and the hybrid network (B). Oscillation period is tabulated for 50 cycles with and without the hybrid network. The CV was calculated and statistical comparisons were made (C) using a Student's t-test for N=7 experiments, yielding a p-value < 0.001. Error bars are reported as standard error.

Activity variability in hybrid networks is not due to a noiseless model

To ensure that reduction in noise variability in our hybrid networks was not due to the introduction of a noiseless computational element, we first tested if the introduction of a noiseless fPRC was necessary to obtain activity variability reduction. We did this by progressively adding extrinsic Gaussian noise to the dynamic clamp calculation of stimulus interval t_R of the synaptic feedback that the biological AB/PD receives, in 20ms increments (Figure 7). A time-scaled output from a Box-Muller algorithm was used to calculate the Gaussian noise. An examination of the resulting changes in activity

variability reduction indicates that noise reduction tends to remain with the addition of at least 20ms of noise. Since the comparable variability level in LP is ~10ms or less, we conclude that activity variability reduction in our hybrid networks is not due to an artificially precise calculation of response interval of synaptic feedback.

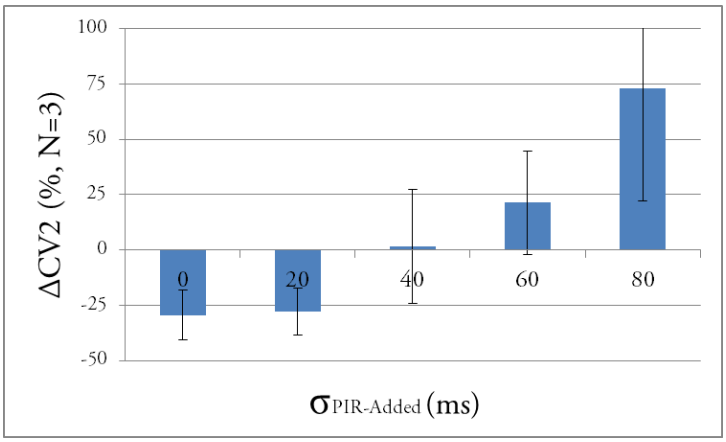

Figure 6. Hybrid network with stochasticity added to VFU response. Shows activity variability reduction in network period, as measured by CV2 (a measure of variability related to the standard deviation and CV) for increasing levels of imposed noise $\sigma_{PIR\text{-}Added}$ in the VFU response interval, implemented with dynamic clamp. A Gaussian noise algorithm was employed in N=3 experiments. Error bars represent SE.

SPECIFIC AIMS

Aim 1: How do phase response dynamics of feedback neurons influence variability of a pacemaker?

Synaptic inhibitory feedback in pattern generating networks has multiple components with properties that are likely candidates for influencing network activity variability. One such component is the synaptic response properties of individual follower/feedback neuron(s), typically quantified by phase response analysis. Theoretical studies have indicated that as phase response curves (PRCs) change in shape, they have the potential to alter the stability of phase locking between two synaptically coupled

neurons, which may have implications for network variability. We utilize extended phase response analysis methods and the dynamic clamp to examine biological feedback neuron phase response properties, then use our findings to construct novel hybrid networks to study the effects of this property on network variability.

Aim 2: Create a theoretical framework for quantifying optimal pacemaker network activity due to phase response properties

In collaboration with the Canavier lab, we sought to develop as simple as possible of a theoretical framework that would quantify how feedback from network interactions transform variable activity of a pacemaker, as represented by a distribution of periods. We succeeded in developing an algorithm that does this for data that is assumed to be generated by a stationary, random process. Since we did not know how valid of an assumption this would be in the pyloric network, we tested how well the network met these criteria using autocorrelation analysis, and found the assumptions were valid in some but not all preparations. In the preparations without statistically significant autocorrelation, we used the dynamic clamp's capability to rapidly construct and deconstruct hybrid networks to test this theory, and found that it was successful in predicting relationships between phase response properties of feedback neurons and network variability. The theory is general enough to have broad potential for impact.

Aim 3: How do pacemaker neuron phase intervals respond to variability on a cycle-by-cycle basis, and does this in turn influence variability?

Another candidate for shaping network variability is in the burst width of feedback neurons, specifically depending on how these intervals react to activity

variability. Much work has shown that activity intervals of neurons in a pacemaking network scale with activity period, but how quickly this scaling occurs or its effect on network activity is not known. We examine intact pyloric network activity burst width, then use insights gained to formulate hybrid networks to test their effects on ongoing network activity.

LAY INTRODUCTION

How do the brain and other neural circuits generate patterns necessary for life that we take for granted, and which when lost or become disordered can be devastating? This has been a driving question for many in neuroscience, and recent advances in technology are helping us address these questions in new ways. But application of new technologies sometimes is fraught with unintended consequences. Biological nervous systems are beautifully rich in complexity and diversity, not only in structure, connectivity, cell types, and neurochemistry, but also in operating principles. Neural communication is at once part discrete and part analog, part additive and part nonlinear, part stochastic and part deterministic. The scientific community creates models of such systems to try to summarize our understanding of them. But what pitfalls might there be in representing such systems as models in inherently less complex, deterministic machines such as computers? Do computers lull us into making certain tradeoffs in our models by the very nature of their operating principles?

In this work I begin to address some of these questions by actually combining biological neurons and computer-based models into one "hybrid" system, which creates a platform for examining these questions that has both the innate stochastic activity of the biology and the determinism of the computer models. I then assess whether similar but

fundamentally different models embedded in this system produce distinct activity. Some models are constructed to reproduce biologically observed responses to stochasticity, while others are constructed to reproduce biologically plausible (but unobserved) alternative responses to stochasticity—where all models are otherwise designed to produce identical activity patterns absent stochasticity. In this way differences observed give us insight into how neurons might be configured and ordered to handle variability in certain ways, and ultimately may help us make more realistic models of networks that attempt to explain network activity by their diverse underlying genetically expressed voltage-sensitive membrane currents.

Of course in order to inform these hybrid networks with what is a biologically observed feature I first had to perform some basic research. The broad range of techniques, theories, and levels of abstraction touched on thus far explains why I chose to study these questions in crustacean neurons. The study of neurons of the crab *C. borealis* may at first seem strange if our interest is in gaining understanding how the brain and nervous system of humans works or is disordered with some pathology, but this system has the unique advantages of having been extensively studied and mapped out over decades of research, exhibiting stereotyped activity and neuron operating principles that is shared with human neurons and nervous systems, being amenable to experimental manipulation, and having been modeled and studied at various levels from the mathematical, to computational, and biomolecular. This creates some real opportunities to cut across disciplines and use multiple perspectives to ask big questions.

CHAPTER 2: FEEDBACK CONTROL OF VARIABILITY IN THE CYCLE PERIOD OF A CENTRAL PATTERN GENERATOR

This chapter was published in 2015 (Hooper et al., 2015).

INTRODUCTION

Central pattern generators drive repetitive motor activity, and both reliability and variability in these networks have been widely studied. Here we study how feedback within circuits mediating the pyloric rhythm of the *Cancer borealis* stomatogastric ganglion (STG) affects variability. The pyloric rhythm is driven by a pacemaker kernel consisting of the anterior burster (AB) neuron electrically coupled to two pyloric dilator (PD) neurons; this electrically coupled group of cells exhibits spontaneous bursting that is driven by AB (for simplicity throughout this chapter we will refer to this combined AB/PD complex as the PD). There is a single chemical feedback synapse onto the pacemaker kernel, an inhibitory synapse from the lateral pyloric (LP) neuron onto the PD neurons (Selverston and Moulins, 1987). Previous work (Nadim et al., 2011) used phase-plane analyses of the oscillator kernel to show that the feedback from LP decreases the variability in the oscillation cycle period of the pyloric rhythm. Another study demonstrated that knowledge of phase resetting information can be used to control periodicity of rhythmic neurons (Stigen et al., 2011), providing a clue that perhaps biological networks utilize phase resetting in some way to govern their rhythmic variability.

The LP neuron is not an intrinsic burster, but rather emits a post-inhibitory rebound (PIR) burst after receiving a burst of inhibitory input from the PD, so it is a

conditional burster (see Fig. 1A2). In a previous study we have shown how the PIR burst can be employed to adapt phase response analysis to such conditional bursters (Sieling et al., 2012), which means that it is now possible to examine the consequences of the interaction between the pyloric network's PD and LP using phase response theory.

In this study, we explore the phase response properties of LP, then provide a general theory of how a feedback element such as LP affects variability in the cycle period of a pacemaker, with the intrinsic period of the pacemaker characterized as a random process. Because some of the variability in pyloric rhythmic activity is often not random but rather is attributable to other processes such as interactions with other CPGs within the stomatogastric nervous system including the gastric mill network (Dando et al., 1973; Mulloney, 1977; Dickinson, 1995; Clemens et al., 1998; Bartos et al., 1999; Thuma and Hooper, 2002; Bucher et al., 2006), we assessed the suitability of this assumption that the pacemaker period is a randomized process by examining the autocorrelation of the pacemaker's intrinsic period. We then use a reduced, hybrid circuit, consisting of an isolated, biological PD pacemaker receiving virtual feedback applied using the dynamic clamp, in order to both test the predictions of this theory and examine the effect of phase response properties of the feedback element on network period variability. The virtual feedback was formulated simply as a latency (tr, or recovery interval) to a burst in the dynamic clamp virtual feedback unit (VFU) as a function of the time elapsed (ts, or stimulus time) since the last burst in the VFU. The tr/ts plot is closely related to the phase response curve (PRC) but has some advantages for hybrid network construction, since it retains temporal information discarded by the PRC, and can be defined for neurons that are not endogenous oscillators such as LP (Sieling et al., 2012).

Moreover, under certain assumptions it lends itself easily to a map of the firing intervals from one cycle to the next (Oprisan et al., 2004; Sieling et al., 2009; Canavier, 2014). Our VFU utilizes tr/ts plots that are based on those observed in the biological LP as well as simple variants in shape to examine the effect of LP's tr/ts curve on network variability.

We were able to predict the distribution of network periods and firing intervals in the PD with feedback, using only 1) the distribution of periods in the isolated PD kernel prior to coupling with the feedback element, 2) the measured recovery intervals for the isolated PD kernel using the VFU, and 3) the latency of the virtual feedback. These results in general were computed numerically. However, we were able to find an analytical solution for one special case; this enabled us to provide an explanation of the effect of feedback on the variability in that case.

METHODS

General experimental methods

Adult *C. Borealis* crabs were obtained via overnight shipping from The Fresh Lobster Company (Gloucester, MA) and maintained in artificial seawater at 10°C. Crabs were anesthetized in ice for 30 minutes prior to dissection. The STG was dissected as described previously (Gutierrez and Grashow, 2009) and pinned out in a Sylgard lined dish containing chilled physiological saline (in mM: 440 NaCl, 11 KCl, 13 $CaCl_2$, 26 MgCl2, 12.4 Trizma base, 5.3 Maleic acid, pH 7.45 @ 13°C). The STG was desheathed and Vaseline wells were formed around the lateral ventricular nerves. All preparations were perfused with physiological saline maintained at 12-14°C. All electrophysiological data were digitized on a Digidata 1322A (Axon Instruments) with an 84μs sampling

interval and recorded using Clampex 9 software (Axon Instruments). Extracellular recordings were made from the wells using stainless steel electrodes inserted into the Sylgard, and signals were filtered and amplified by an A-M Systems Model 1800. Intracellular recordings were made with an Axoclamp 2B amplifier (Axon Instruments) in discontinuous current-clamp mode using glass microelectrodes (10-20 MΩ) filled with a solution of 0.6 M K_2SO_4 and 20 mM KCl. PD neurons were identified with standard procedures for *C. borealis* (Selverston and Moulins, 1976; Harris-Warrick, 1992) then pharmacologically isolated from glutamatergic synaptic input from LP using physiological saline containing 10^{-5} M Picrotoxin (PTX, Sigma-Aldrich) (Bidaut, 1980). LP neurons were isolated from synaptic input using a combination of PTX and photoinactivation of both identified PD neurons to eliminate their cholinergic input onto LP (Miller and Selverston, 1979). This was accomplished using glass microelectrodes backfilled with Alexa Fluor 568 hydrazide (10 mM in 200 mM KCl, Invitrogen) to inject -5 nA DC current into a PD soma for 20-30 minutes. The filled cell was then illuminated with a Leica EL6000 and MZFLIII using a TXR filter set for 10-15 minutes. Dynamic clamp (Dorval et al., 2001) protocols were programmed in house and run with an update rate of 50 μs on a computer with a NI PCI-6052E data acquisition card (National Instruments). Within these dynamic clamp protocols, we defined burst onset of all rhythmic biological membrane voltage traces to occur when the rising phase of the slow oscillation crossed a voltage threshold. This threshold was chosen so that it would be crossed as the rising slow oscillation was steepest to give maximum tolerance to baseline drift, and the slow oscillation trace was isolated from spikes by filtering the membrane voltage trace according to $V_{filt}(t + \Delta t) = V_{filt}(t) + [V_m(t + \Delta t) - V_{filt}(t)]\Delta t/\tau_{filt}$,

where V_{filt} is the filtered membrane voltage, V_m is the unfiltered membrane voltage, Δt is the dynamic clamp time step of 50 μs , and τ_{filt} = 50 ms. Analysis of all recordings was performed offline in Spike2 (Cambridge Electronic Design).

tr/ts curve measurement and estimation

The interval between burst onset of a neuron and the onset of synaptic input from another neuron is the stimulus interval (ts_x) for each neuron, x = AB/PD or LP. The corresponding interval between input onset and the next burst is defined as the recovery interval (tr_x). We define the functions $tr_x = g_x(ts_x)$ to quantify the dependence of tr_x on ts_x. Using dynamic clamp, these relations are measured experimentally using a multiple-pulse PRC protocol based on the functional PRC or fPRC (Cui et al., 2009; Sieling et al., 2012), but performed assuming no adaptation or second order resetting, such that tr/ts curves obtained are equivalent to those obtained from a PRC protocol (which we will refer to as a single-pulse PRC). These assumptions are reasonable due to results from previous studies that showed negligible second order resetting in PD for artificial inhibitory inputs within a biologically plausible parameter range, except for very early or late stimulus intervals that are not important to the alternating firing patterns of our networks (Oprisan et al., 2004; Maran et al., 2011). For oscillatory neurons our protocol proceeds by first applying an initial hyperpolarizing stimulus to more closely simulate the oscillation observed in the coupled network, and discarding the initial recovery interval tr[0], then repeatedly presenting a sequence of artificial synaptic inputs at a given stimulus interval (N=10-13 repetitions). Stimulus intervals of 20 equally spaced increments of the estimated intrinsic network period were measured in random order

(Fig. 7A1). Measurement of tr/ts curves for LP proceeds in the same way (Fig. 7A2), but since LP is not an endogenous bursting oscillator, the initial hyperpolarizing stimulus serves to evoke a rebound burst, which can then be used to determine proper stimulus interval for the next burst cycle (Sieling et al., 2012). The resulting response intervals tr[1]-tr[N] were analyzed for mean and standard deviation at each stimulus interval, and the results sorted by stimulus interval for plotting as a tr/ts curve (Figs. 7B1, 7B2). Finally, these 20 points were fit with smoothing splines under tension (with weights inversely proportional to standard deviation as in (Reinsch, 1967) for use by theoretical methods.

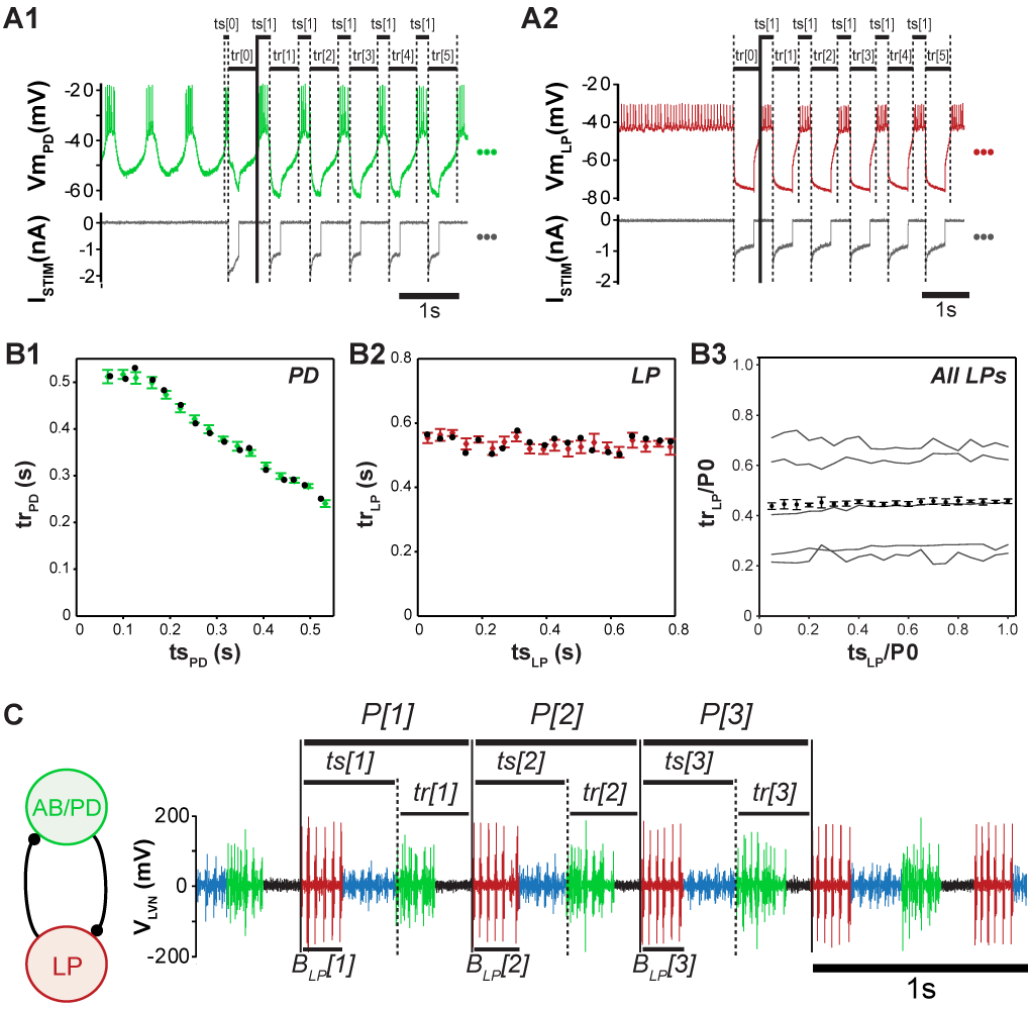

Figure 7. Measurement of tr/ts curves and firing intervals in the pyloric network. (A1) tr/ts curve measurement from intracellular PD procedes by repeatedly stimulating with an artificial synaptic input generated with dynamic clamp at a given *ts*, then repeating for each *ts* to be measured. (A2) tr/ts measurement in nonbursting LP (B1) Resulting response intervals are tabulated into the tr/ts curve for PD, exhibiting typical tr/ts curve shape for PD (green points are mean±SD for each *ts*, black dots are the first response intervals recorded at each new stimulus interval whose similarity to average values are indicative of negligible second order resetting). (B2) tr/ts curve tabulated from LP (red points are mean±SD for each *ts*, black dots are the first response intervals recorded for each new stimulus interval, suggesting that LP also exhibits negligible second order "resetting"). (B3) LP exhibits a flat tr/ts curve, corresponding to a constant response interval independent of stimulus interval (N=5 animals). Thin black lines show individual tr/ts curves as linearly interpolated means, normalized by each pyloric network's intrinsic period P0. Red points show the mean tr/ts curve (mean±SE, adjusted for pairwise comparisons). (C) Extracellular voltage trace showing stereotypical activity of the pyloric pacemaker unit AB/PD (light green, one AB and two PDs) and follower neurons LP (red), which are connected with reciprocal inhibitory synapses and burst in a periodic firing pattern lead by AB/PD. PY follower neurons (blue spikes) are also present in the pyloric circuit but their effect on LP is ignored. LP stimulus intervals ($ts[i]$) measure timing of synaptic input from AB/PD relative to the start of each cycle period $P[i]$, and response intervals ($tr[i]$) measure the corresponding timing of LP's next burst relative to synaptic input from AB/PD. Because LP's tr/ts curve was found to be flat in (B), the mean LP response interval $\overline{tr}$ measured in extracellular activity is an estimate of LP's tr/ts curve. Periods, firing intervals, and LP burst durations B_{LPi} were also measured and averaged to inform our hybrid networks such that they operate with pyloric-like activity.

The values of the parameter of the artificial synaptic input used to measure the tr/ts curve of PD neurons including conductance, duration, and reversal potential were identical in each preparation to the parameter values selected for use in the hybrid networks (see *Hybrid Networks*). For LP, the applied artificial synaptic input had conductance set to 100-150nS, a fixed duration proportional to each preparation's average PD burst width as measured prior to intracellular impalement in 40 cycles of the extracellular recording of intact pyloric network activity, and a reversal potential of -90mV.

Hybrid Networks

We constructed hybrid networks by coupling a biological PD to a dynamic clamp element that serves to replace feedback from LP to PD (Fig. 8A, we refer to this dynamic clamp element as a virtual feedback unit [VFU] to avoid confusion with a biological LP). The feedback from the VFU was simulated in the simplest form possible, as a linear tr/ts curve of arbitrary slope that responds to burst onset of PD, where the VFU's output burst duration and average activity phase when coupled to PD are chosen to approximate LP activity.

We determined LP's mean activity as follows: prior to intracellular impalement, 40 extracellularly recorded cycles of the intact pyloric network were analyzed to obtain measures of mean LP stimulus and response intervals $\overline{ts_{LP}}$ and $\overline{tr_{LP}}$, mean LP burst duration $\overline{B_{LP}}$, and mean network period $\overline{P_{net}}$ (Fig. 7C). So that these parameters could be scaled to a hybrid network of any period to mimic the phase maintenance present in the intact pyloric network (Hooper, 1997a, 1997b; Bucher et al., 2005; Soofi et al., 2012), corresponding phase intervals were then calculated as $\overline{\phi s_{LP}} = \overline{ts_{LP}}/\overline{P_{net}}$, $\overline{\phi r_{LP}} = \overline{tr_{LP}}/\overline{P_{net}}$, and LP duty cycle $\overline{DC_{LP}} = \overline{B_{LP}}/\overline{P_{net}}$.

We then set the VFU's burst width interval to a fixed value based upon the observed LP burst duty cycle, $B_{VFU} = \overline{DC_{LP}} \cdot P_0$, where P_0 is the mean period of the isolated PD prior to the formation of a hybrid network.

We then determined the parameters of each VFU tr/ts curve equation necessary to reproduce average phasing of LP across all tested tr/ts curve slopes. This maintenance of average phasing is necessary in order to study variability separately from effects on the average period. For phase locked networks, the cycle period is the sum of the mean

stimulus intervals in the two neurons, or the sum of the mean stimulus and response intervals in a single neuron (Weaver and Hooper, 2003; Mamiya and Nadim, 2004), and as a result our hybrid network average period will be dependent upon the corresponding intervals $ts^*_{PD} = tr^*_{VFU}$ and $tr^*_{PD} = ts^*_{VFU}$, where an asterisk indicates a steady-state fixed point. Graphically this fixed point is located at the intersection of the plots of the tr/ts curve for the PD and the inverse of the tr/ts curve for the VFU at $(ts^*_{PD}, tr^*_{PD}) = (tr^*_{VFU}, ts^*_{VFU})$ (fig. 8C). To keep this fixed point independent of VFU tr/ts curve slope we modeled the VFU's tr/ts curve as family of linear functions in point-slope form that each contain the fixed point (tr^*_{VFU}, ts^*_{VFU}), so obtain $tr_{VFU} = g_{VFU}(ts_{VFU}) = m \cdot (ts_{VFU} - ts^*_{VFU}) + tr^*_{VFU}$; where m is the slope. The system's fixed point (tr^*_{VFU}, ts^*_{VFU}) was estimated as $(P_0 \cdot \overline{\Phi r_{LP}}, P_0 \cdot (1 - \overline{\Phi r_{LP}}))$ by recognizing that $P_{net} = ts_{VFU} + tr_{VFU}$, and substituting the observed LP response phase scaled by P_0 for tr^*_{VFU}, where P_0 is used as an estimate of P_{net}. We varied the slope (presented in randomized order) from -0.4 to +1.0 by increments of 0.2 (fig. 8C).

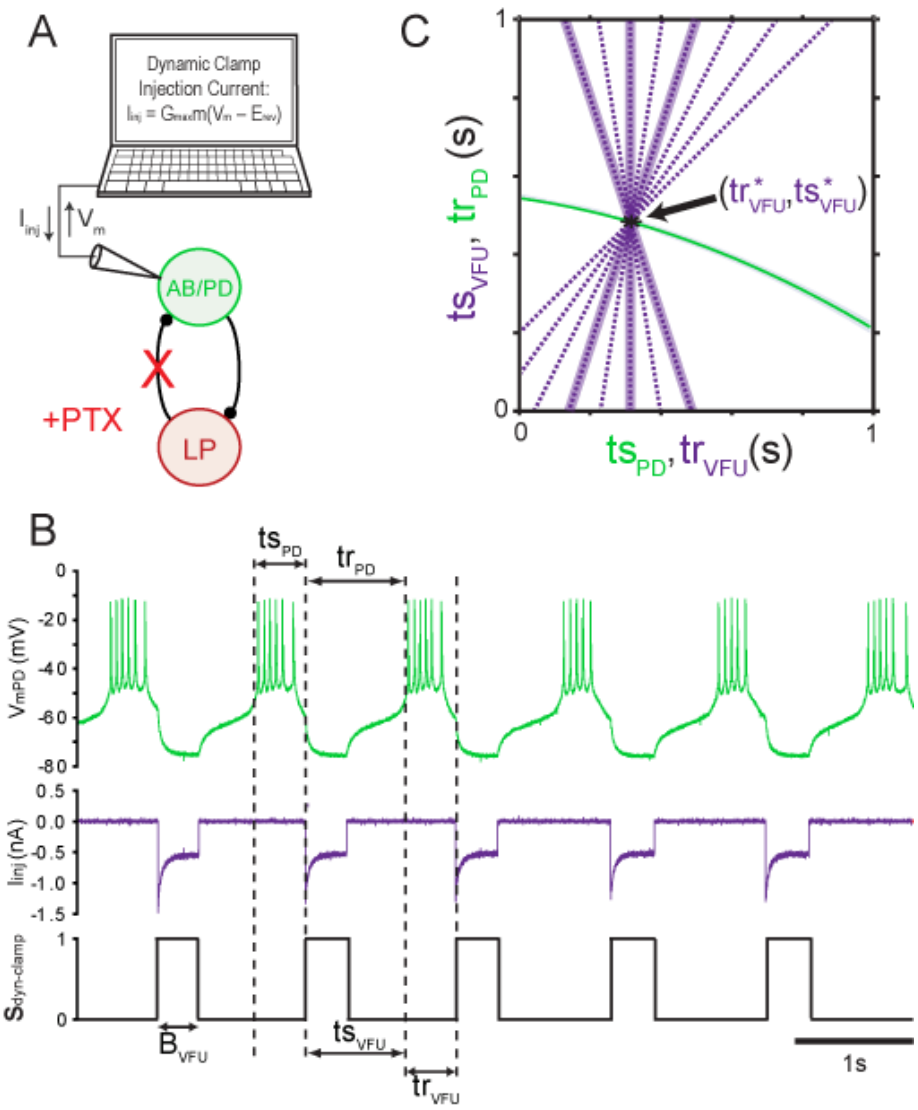

Figure 8. Hybrid network protocol for a biological PD and a virtual feedback unit (VFU) that replaces LP. Hybrid networks are established by interfacing a pharmacologically isolated PD with the dynamic clamp (A). The dynamic clamp simulates an LP-like VFU and its synaptic feedback to PD where the response interval tr_{VFU} is a delay indexed from the beginning of the burst in PD (B) and a function of the elapsed stimulus interval ts_{VFU}, implemented explicitly as a tr/ts curve (purple dashed curves, C),. Once tr_{VFU} has elapsed the dynamic clamp initiates an inhibitory square conductance pulse of fixed duration B_{VFU}, set to mimic LP's burst duration as was measured from the intact pyloric network (see Fig. 1C). The VFU tr/ts curves are linear models with slopes m (tested from -0.4 to +1.0 by increments of 0.2) that are set to maintain a consistent fixed point (tr^*_{VFU}, ts^*_{VFU}) across slopes and approximate pyloric activity phases (see text). Highlighted tr/ts curves: m = -0.4, 0, and +0.4.

Finally, we neglect synaptic plasticity and assume that all maximal synaptic conductances in the hybrid network are constant. The VFU to biological PD synapse is constituted by a 50nS virtual conductance with instantaneous activation injected into PD using a reversal potential of -90mV. Both selected values of conductance and reversal potential were based upon previous voltage clamp measurements from this synapse (Thirumalai, 2002; Archila and Prinz, 2012; Archila, 2013). The PRC of the AB/PD complex is not very sensitive to changes in the strength of synaptic input (Prinz et al., 2003b) above 50 nS. The PD to VFU synapse is implicit in the tr/ts curve for the VFU and was calibrated by the biological PD to LP synapse of the intact pyloric network.

Statistics

Inferential statistics were performed using the analytics software package SPSS 21 (IBM). In all statistical tests the same rhythm features (period and SD) were measured under all conditions of tr/ts curve slope from the same experimental preparation, so they were analyzed as repeated measures datasets. One-way repeated measures analysis of variance (rANOVA) was performed on experimental data to determine if slope had an effect, and if an effect was present, planned comparisons were performed to test the significance of the VFU's tr/ts curve with m=0. Standard errors were calculated as for repeated measures designs (O'Brien and Cousineau, 2014). Autocorrelation functions were analyzed in MATLAB using 20 lags and a sequence of 200 cycle periods of each isolated PD. 95% confidence intervals for the autocorrelation functions were estimated in the standard manner as $\pm 1.96/\sqrt{n}$, where n is the number of cycle periods in each sequence.

Theoretical Methods

The theoretical methods are based on the following assumptions. 1) The oscillator and the feedback element fire in an alternating pattern when coupled. This is a strong assumption that requires there never be consecutive bursts in one cell before the other has a chance to fire. 2) The response of each cell to an input from the other cell is characterized by measuring the time between the receipt of an input until the cell fires next (the recovery interval tr) as a function of the time elapsed since the cell fired last (the stimulus interval) $tr_x = g_x(ts_x)$. Using this curve requires three assumptions: 2a) When coupled in the circuit each network element has the same response to input from its partner as it does in isolation when the tr/ts curve is measured. This assumes burst duration is constant, and changes in burst duration are ignored in our analysis. 2b) The coupling is pulsatile so that the effects of an input are complete within one cycle and are not cumulative (no adaptation). 2c) Second order phase resetting is assumed to be zero, meaning that only the length of the cycle that contains the input is affected, and not any subsequent cycles.

Fig. 9A shows how a map can be constructed for subsequent intervals given an initial condition, for example, a PD recovery interval for hybrid network cycle n, $tr_{PD}[n]$. Under the assumption of an alternating firing pattern, the stimulus interval in one neuron is equal to the recovery interval in the other, so we can get the next stimulus interval in the VFU using $ts_{VFU}[n+1] = tr_{PD}[n]$. We can then obtain the next recovery interval in the VFU using the tr/ts curve for the VFU $tr_{VFU}[n+1] = g_{VFU}(ts_{VFU}[n+1])$. In order to visualize these steps, we can plot the tr/ts curve information for the two neurons

with $g_{PD}(ts_{PD})$ and ${g^{-1}}_{VFU}(tr_{VFU})$ on the y-axis. The inverse is used in order to get equal quantities—stimulus and recovery interval pairs in partner cells—on the same axis. The map described so far can be visualized in the plane shown in Fig. 9B as the horizontal arrow leading from the point $(ts_{PD}[n], tr_{PD}[n])$ to the point $(tr_{VFU}[n+1], ts_{VFU}[n+1])$. Finally, we apply the alternating firing criterion $ts_{PD}[n+1] = tr_{VFU}[n+1]$ and use the tr/ts curve for PD to get $tr_{PD}[n+1] = g_{PD}(\, ts_{PD}[n+1])$. These final steps can be visualized as the vertical arrow leading from the point $(tr_{VFU}[n+1], ts_{VFU}[n+1])$ to the point $(ts_{PD}[n+1], tr_{PD}[n+1])$ in Fig. 9B. Substitution of the results from the previous steps into the final step allows each recovery interval in PD to be calculated from the previous interval as follows:

$$tr_{PD}[n+1] = g_{PD}\big(g_{VFU}(tr_{PD}[n])\big) \quad (1)$$

We now introduce assumption 3 and 4 in addition to the other assumptions described above. 3) We assume that the intrinsic period of the PD neuron is not constant, but rather is drawn from a smooth and continuous stationary distribution $\rho_{P_{PD}}(P_{PD})$ that can be measured. In order to keep theoretical result as general as possible, we do not assume any specific distribution for $\rho_{P_{PD}}(P_{PD})$, but instead the assumption of a constant distribution allows us to estimate $\rho_{P_{PD}}(P_{PD})$ from a recording just prior to hybrid network coupling. The measured histogram is used to solve integral equation (6) numerically. We assume that the period is a random process that draws from this distribution with no dependence on previous values (history-independent or memoryless).

We therefore redefine the map by incorporating a random process $P_{PD}[n]$ for the intrinsic period of PD sampled once per cycle.

$$tr_{PD}[n+1] = g_{PD}(g_{VFU}(tr_{PD}[n]), P_{PD}[n]) \quad (2)$$

4) We further assume that the tr/ts curve scales with changes in period (this assumes the PRC is invariant with respect to frequency). Thus both ts_{PD} and tr_{PD} are scaled by the factor $P_{PD}[n]/P_0$, where $P_{PD}[n]$ is the period of the present cycle and P_0 is the estimated mean period at the time the curve was generated, such that:

$$tr_{PD}[n+1] = g_{PD}(ts_{PD}[n], P_{PD}[n]) = (P_{PD}[n]/P_0)\, g_{PD}(ts_{PD}[n] P_{PD}[n]/P_0)$$

We checked this strong assumption in a direct experiment described in Experimental verification in *Results* and Fig. 10.

The distribution of intrinsic periods produces a continuous family of tr/ts curves (Fig. 9C), shown for a representative neuron with the thickness of line proportional to the probability of a given period and its associated tr/ts curve. Note that in the hybrid circuit constructed with the dynamic clamp (see *Experimental Methods*), the tr/ts curve for the VFU is held constant. Therefore any given point on the tr/ts curve of the VFU will map onto different tr/ts curves for PD on different cycles if the period is variable (Fig. 9D).

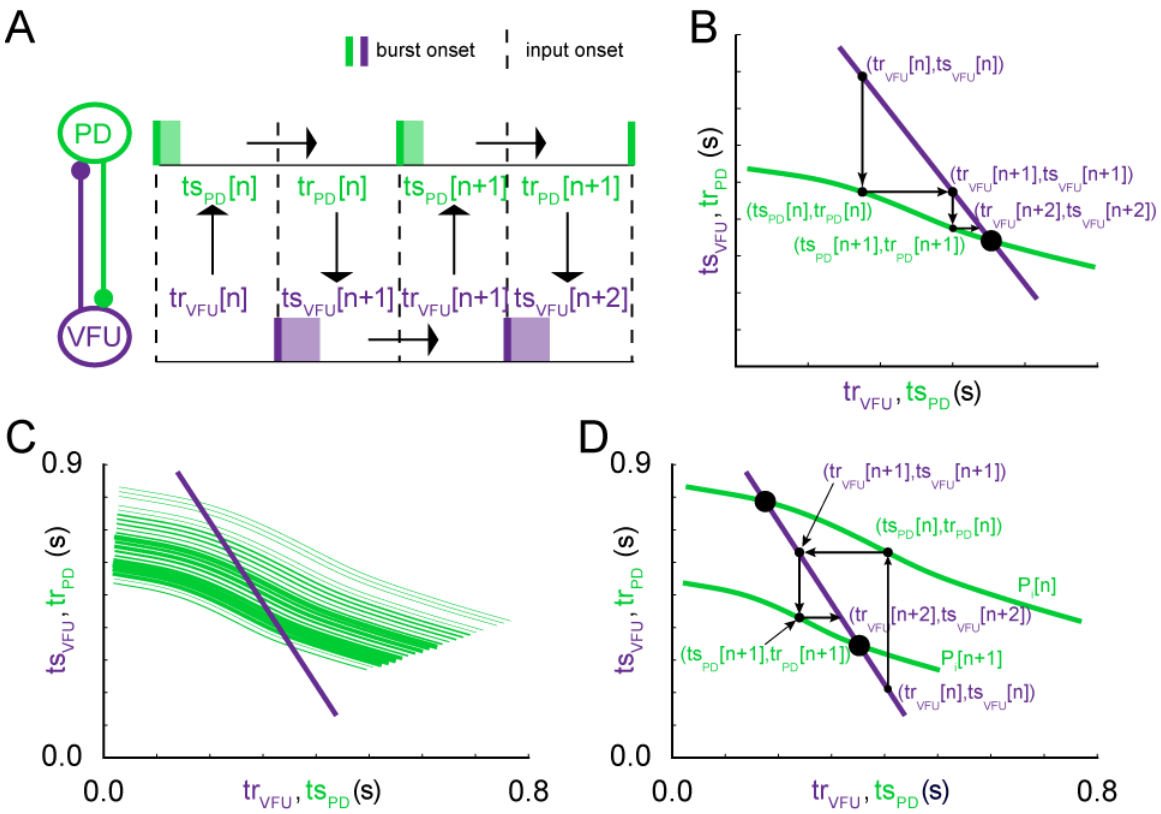

Figure 9. Map of the firing intervals. (A) The schematic shows the sequential prediction (arrows) of subsequent firing intervals in an alternating firing pattern given an arbitrary initial condition. Given that we have knowledge of the tr/ts relationship g_x for both neurons, the recovery interval in one neuron becomes the stimulus interval for the partner neuron. (B) The dependence of tr_{PD} on ts_{PD} (dark purple curve) and of tr_{VFU} on ts_{VFU} (light green curve) are plotted with the axes swapped for the purple curve in order to plot stimulus intervals from one neuron on the same axis as recovery intervals from the other neuron. In this space, horizontal arrows in B correspond to downward arrows in A, and vertical arrows in B correspond to upward arrows in A. The small dots indicate iterations of the firing interval, and the large dot indicates a stable attracting fixed point. (C) A representative distribution of the dependence of tr_{PD} on ts_{PD} (green curves) at different intrinsic periods, with the probability of exhibiting a period increasing with the thickness of the curve. (D) The same map as in B except the intrinsic period of PD changes randomly in each cycle.

RESULTS

Theoretical results

Our objective is to predict the distribution of the network periods $\varrho_{P_{net}}(P_{net})$ in the hybrid circuit consisting of a pacemaker with feedback, using the known distribution

of intrinsic periods $\rho_{P_{PD}}(P_{PD})$ measured in an uncoupled PD neuron and the known functions g_{PD} and g_{VFU} (see *Methods*). If the theoretically stationary distribution $\varrho^*_{tr_{PD}}$ of the recovery intervals in PD is found, the distribution of the network periods can then be obtained by finding each independent way of arriving at a given P_{net} . These independent ways are found by plugging each possible pair of $\tau = tr_{PD}$ and $p = P_{PD}[n]$ within the range of these values ($\Omega(tr_{PD})$ and $\Omega(P_{PD})$ respectively) into the expression $P_{net} - g_{PD}(g_{VFU}(\tau), p) - g_{VFU}(\tau)$ that is inside the delta function in *Eq. 3*. Then the probability of each P_{net} is found by summing the probabilities $\varrho^*_{tr_{PD}}(\tau)\varrho_{P_{PD}}(p)$ of each independent way to arrive at that P_{net}.

$$\varrho_{P_{net}}(P_{net}) = \iint_{\Omega(tr_{PD})\Omega(P_{PD})} \varrho^*_{tr_{PD}}(\tau)\varrho_{P_{PD}}(p)\delta(P_{net} - g_{PD}(g_{VFU}(\tau), p) - g_{VFU}(\tau))d\tau\, dp \quad (3)$$

Therefore, as an intermediate step, we attempted to determine the theoretical stationary distribution of the recovery intervals in PD, $\varrho^*_{tr_{PD}}(tr_{PD})$. We took advantage of a trivial fact that for any set of initial conditions and any time series of intrinsic period for PD, the observation that in the experimentally recorded time series, the distribution of $tr_{PD}[n+1]$ is approximately equal to that of $tr_{PD}[n]$ for large n, because those distributions are obtained from sets which consist of n-1 identical elements.

$$\begin{array}{ccccccccccccc} tr_{PD}[0] & & tr_{PD}[1] & & tr_{PD}[2] & & tr_{PD}[3] & \dots & tr_{PD}[n] & & & \Rightarrow & \varrho_{tr_{PD}(tr_{PD}[n])} \\ & \searrow & & \searrow & & \searrow & & & & \searrow & & & \\ & & tr_{PD}[1] & & tr_{PD}[2] & & tr_{PD}[3] & \dots & tr_{PD}[n] & & tr_{PD}[n+1] & \Rightarrow & \varrho_{tr_{PD}(tr_{PD}[n+1])} \end{array}$$

The arrows indicate that as n goes to infinity, the distribution of the sample values approaches the theoretical distribution from which the sample was drawn. In the case of a stationary or quasi-stationary distribution, this gives us a self-consistency criterion for the distribution of recovery intervals in PD:

$$\varrho^*_{tr_{PD}}(tr_{PD}[n+1]) = \varrho^*_{tr_{PD}}(tr_{PD}[n]) = \varrho^*_{tr_{PD}}(tr_{PD}) \quad (4)$$

Since we know the dependence of each recovery interval in PD upon the previous one, we need to find the distribution of $\varrho^*_{tr_{PD}}(tr_{PD})$ which maps to itself by finding each independent way of arriving at a given tr_{PD}. These independent ways are found by plugging each possible pair of $\tau = tr_{PD}[n]$ and $p = P_{PD}[n]$ within the range of these values ($\Omega(tr_{PD})$ and $\Omega(P_{PD})$ respectively) into the expression $g_{PD}(g_{VFU}(\tau), p)$ that is inside the delta function in *Eq. 5*. Then the probability of each arriving at a given tr_{PD} is found by summing the probabilities $\varrho_{tr_{PD}}(\tau)\varrho_{P_{PD}}(p)$ of each independent way to arrive at that $tr_{PD}[n+1]$.

$$\varrho^*_{tr_{PD}}(tr_{PD}) = \iint_{\Omega(tr_{PD})\Omega(P_{PD})} \varrho^*_{tr_{PD}}(\tau)\varrho_{P_{PD}}(p)\delta\big(tr_{PD} - g_{PD}(g_{VFU}(\tau), p)\big)d\tau\, dp \quad (5)$$

Note that the use of $\varrho^*_{tr_{PD}}(\tau)$ on the right hand side of *Eq. 5* implies that we need to know the distribution of recovery intervals over the space $\Omega(tr_{PD})$ of possible tr_{PD} values in order to find the distribution. However, we do not actually need to know this

distribution *a priori* because we can resolve the integrative equation (5) iteratively, starting from a random distribution $\varrho^{0}_{tr_{PD}}(tr_{PD})$ (Fig. 10A) in the right-hand side of equation (5). We then obtain $\varrho^{1}_{tr_{PD}}(tr_{PD})$ (Fig. 10B) on the left-side of equation (5), and repeat for k iterations until $\varrho^{k}_{tr_{PD}}(tr_{PD})$ converges to the desired steady state distribution $\varrho^{*}_{tr_{PD}}(tr_{PD})$ (Fig. 10D) that satisfies the self-consistency criterion (4) above. The distribution converges if $g_{PD}(g_{VFU}(\tau), p)$ is smooth and monotonic (Press et al., 2007). The integral was approximated by binning the tr_{PD} values into equally spaced bins, and recalculating the bins after each iteration, so that we obtain a histogram that approximates the theoretical distribution. In Fig. 10 we illustrated this process, but instead of plotting tr directly, we plot the associated network period using $Pnet = g_{PD}(g_{VFU}(\tau), p) + g_{VFU}(\tau)$ for direct comparison with the experimental data (see Fig. 10D).

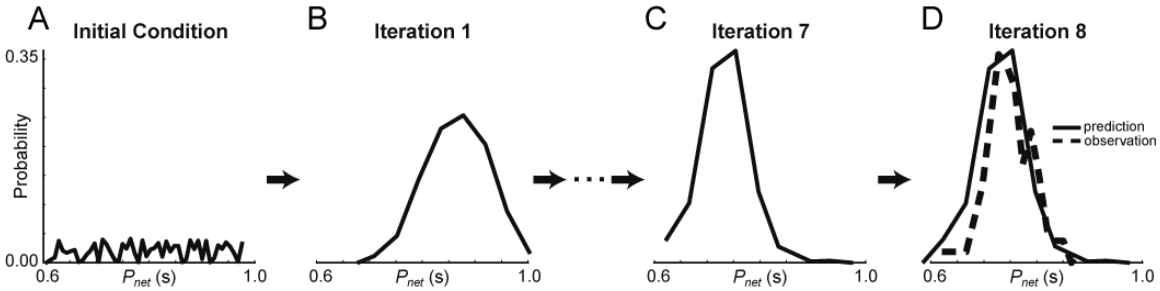

Figure 10. Convergence of the distribution of the recovery intervals $\varrho_{tr_{PD}}(tr_{PD})$ yields iterative convergence for periods $\varrho_{P_{net}}(P_{net})$ in PD. (A) The map $\varrho^{k}_{tr_{PD}}(tr_{PD}) \Rightarrow \varrho^{k+1}_{tr_{PD}}(tr_{PD})$ was randomly initialized at k=0, and used to produce the random distribution of network periods shown here. (B) After a single iteration (k=1) the distribution shows a distinct peak. **(**C) At k=7, the distribution reaches steady state. (D) The histogram for k=8 is indistinguishable from that for k=7 in C, indicating that the algorithm has converged to a steady state distribution. Moreover, there is a strong resemblance between the calculated histogram (solid curve), and the actual experimentally observed histogram (dashed curve).

Experimental verification

Using hybrid networks constructed based on the rhythmic crustacean pyloric network, we explored how the distribution of the network period responds to simple changes in phase response properties of a VFU, which serves the same role in providing feedback to the pacemaker PD as LP does in the intact pyloric network. This hybrid system then provides rhythmic activity against which our theoretical predictions can be compared. Prior to pharmacological isolation of PD, the intact pyloric network preparations used for these purposes displayed mean periods of 887±196ms (mean±S.D.; n=9 preparations), and were all within the 0.5-2.0Hz cycle frequency range typically observed in this system. The average dispersion of period in each intact preparation as measured by standard deviation was 15±4ms. Average LP burst duration was 217±66ms, representing a burst duty cycle of 0.243±0.040. Following pharmacological isolation of PD, the PD neurons then displayed mean periods of 758±116ms, and dispersion of 39±19ms.

We first tested the assumption that the tr/ts curve shape was relatively preserved as the period varied in our system. We began by repeatedly measuring the tr/ts curve over time of a PD neuron which displayed drift in intrinsic period (Fig. 11A1), then normalized each resulting curve by the average intrinsic period P_0 observed immediately prior to tr/ts measurement (Fig. 11A2), revealing that the tr/ts curve shape is relatively conserved as period changes. Similar conservation of tr/ts curve shape was observed when we altered the PD period over a 3x range by sweeping preparation temperature (Tang et al., 2010; Soofi et al., 2014) between 10°C and 20°C (data not shown). Then we verified that second order resetting was negligible in both PD and LP by comparing the

first recovery interval tr[1] with the average of the train tr[1]-tr[N] in Figure 7B, and found them to be indistinguishable.

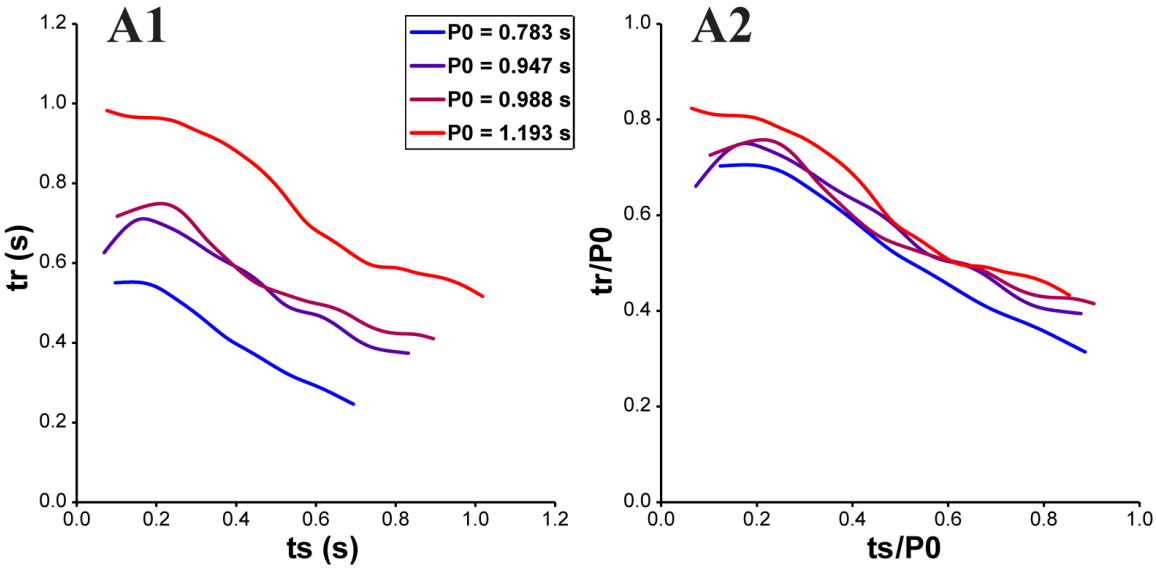

Figure 11. Experimental test of the assumed invariance of the tr/ts curve. (A1) The tr/ts curve of one PD was measured four different times over multiple hours, during which an increase in intrinsic period occurred. (A2) Plots of the normalized curves show that tr/ts curve shape is largely invariant with the observed changes in intrinsic PD period.

Next we tested our assumption that the PD oscillation periods do not depend on previous values (are memoryless) using autocorrelation analysis (Fig. 12A) of 200 consecutive unperturbed oscillation cycles of the isolated PD (Fig. 12B). Of n=33 separate preparations analyzed, we found that presence of autocorrelation varied between animals. Roughly half (16/33 = 48.5%) of preparations displayed no statistically significant autocorrelation (Fig. 12A1), while half (17/33 = 51.5%) displayed statistically significant autocorrelation (Fig. 12A2), including one preparation that show a strikingly regular cycle-to-cycle alteration between two different period values (pink in Fig. 12A2 and 12B2). Consequently we will only consider preparations for which there is no significant autocorrelation for use in theoretical predictions, because only those preparations fulfill the assumptions of our theoretical prediction method.

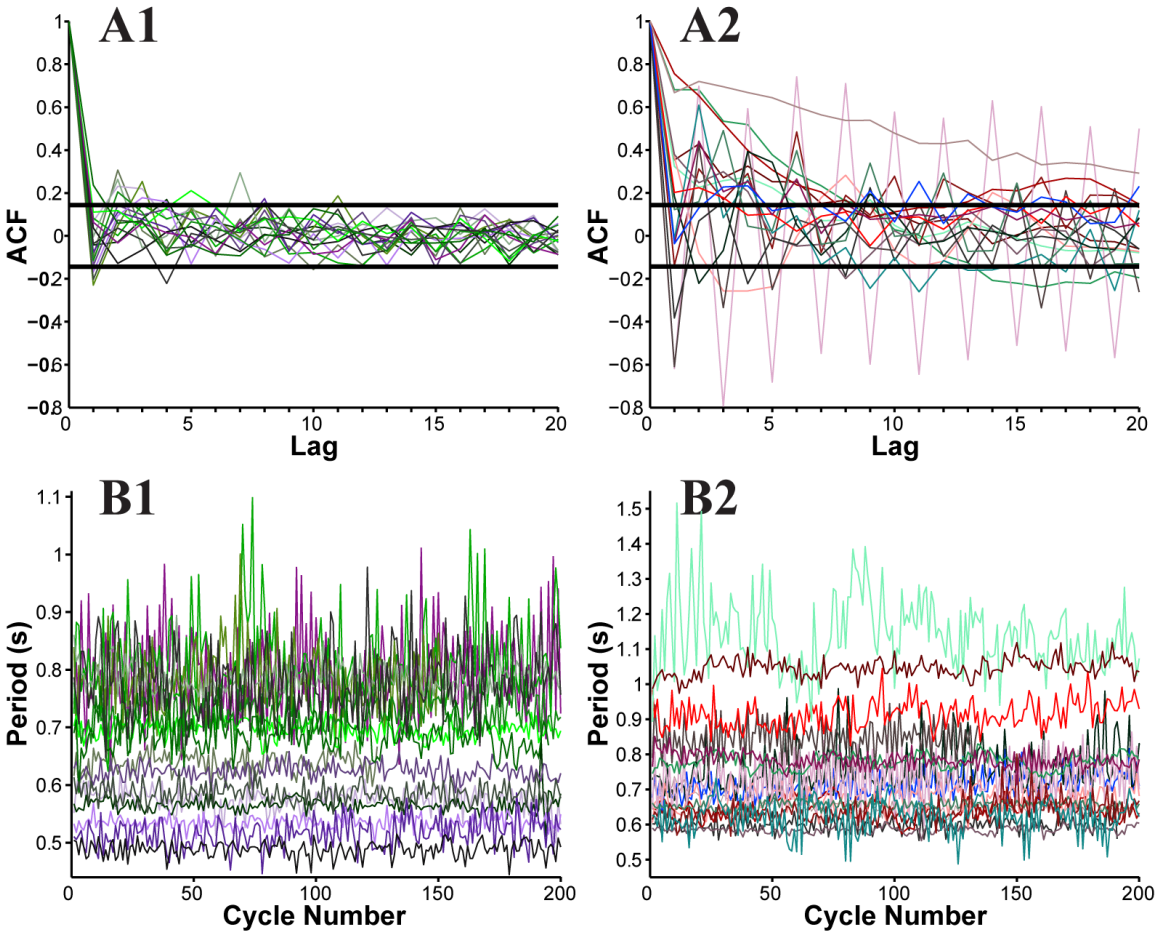

Figure 12. Experimental test for the presence of memory in the intrinsic period of PD. (A) Pearson's autocorrelation function for 33 different preparations (N=200 cycle periods each) indicates (A1) lack of significance autocorrelation in 16 preparations but (A2) significant autocorrelation of varying strengths present in 17 preparations (A2). 95% confidence intervals marked by black horizontal bars. (B) Individual recordings underlying these autocorrelations are summarized in plots of their cycle period progression over time beneath their respective autocorrelation plots.

In the intact pyloric network, PD receives synaptic feedback from LP. In the hybrid networks, we implemented an approximation of this feedback using an explicit dynamic clamp implementation of the linear tr/ts curves exhibited by LP in response to synaptic input: $tr_{VFU} = g_{VFU}(ts_{VFU}) = m \cdot (ts_{VFU} - ts^*_{VFU}) + tr^*_{VFU}$; where m is the slope and (tr^*_{VFU}, ts^*_{VFU}) is the system's estimated fixed point (see *General Experimental*

Methods). This approximation allowed us to easily manipulate the parameters of the feedback. For these networks, the integral equation (5) can be rewritten as follows:

$$\varrho^*_{tr_{PD}}(tr_{PD}) = \iint_{\Omega(tr_{PD})\Omega(P_{PD})} \varrho^*_{tr_{PD}}(\tau)\varrho_{P_{PD}}(p)\delta\big(tr_{PD}[n+1] - g_{PD}(m\cdot(\tau - ts^*_{VFU}) + tr^*_{VFU}, p)\big)d\tau\, dp \quad (6)$$

The resulting hybrid networks allow us to validate our theoretical methods in networks with a variety of tr/ts curves for which the resulting distribution of periods may vary systematically. The stability criterion for a network of two neurons described by tr/ts curves coupled with fixed delays is $-1 < g'_{PD}(ts^*_{PD}) \cdot g'_{VFU}(ts^*_{VFU}) < 1$, as derived by calculating the eigenvalues of the map in *Eq. 1* when a small perturbation is applied to the firing times as in (Cui et al., 2009), where a prime indicates the slope of the tr/ts curve and asterisks indicate values at the fixed point. In the map we have plotted in Fig. 8C and Figs 9B-D, $g_{PD}(ts^*_{PD})$ is plotted versus the inverse function $g^{-1}_{VFU}(ts^*_{VFU})$. An inverted tr/ts curve with a slope of zero is plotted as a vertical line. Using the coordinates at the intersection of the curves, this fixed point is stable if the absolute value of the slope of the purple curve $g^{-1\prime}_{VFU}(ts^*_{VFU})$ is greater than that of the green curve $g'_{PD}(ts^*_{PD})$ (see derivation in section 2 of Supporting Information Text in Thounajam et al., 2014).

Measuring the biological LP's tr/ts curve in n=5 preparations (Fig. 7B3) indicated that the biological LP has a tr/ts curve with a slope of approximately zero, similar to those in lobster (*Homarus americanus*) (Sieling et al., 2012).

We then constructed hybrid networks experimentally and assessed the impact of VFU tr/ts curve slope on the distribution of network period using inferential statistics. The effect of slope on mean period of the distributions was assessed with a one-way rANOVA and not significant, F(7,56)=2.28, p=0.12 (Fig. 13A). However, there was a significant effect of slope on variability as assessed by a one-way rANOVA of the standard deviation of the distributions of period, F(7,56)=6.83, p<0.001. Further analysis by planned comparisons reveals that the hybrid network with a VFU of slope zero ($m = 0$) had significantly lower variability compared to all other nonzero slopes tested (Fig. 13B), each representing a large effect size, $m = -0.4$: t(8)=-3.49, p=.008, r=0.78; $m = -0.2$: t(8)=-2.62, p=0.031, r=0.68; $m = +0.2$: t(8)= -2.43, p=0.041, r=0.65; $m = +0.4$: t(8)=-2.69, p=0.028, r=0.69; $m = +0.6$: t(8)=-2.34, p=0.048, r=0.64; $m = +0.8$: t(8)= -3.11, p=0.014, r=0.74; $m = +1.0$: t(8)= -4.22, p=0.003, r=0.83.

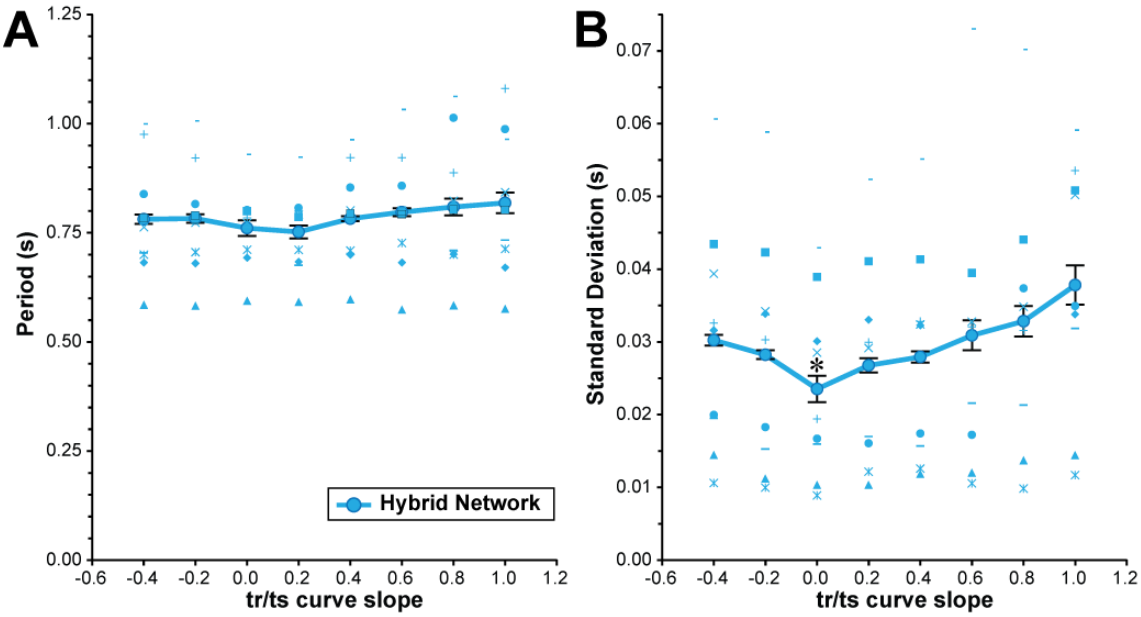

Figure 13. Experimental change in hybrid network variability with change in tr/ts curve slope. Hybrid network period (A) and variability (B, as standard deviation) were assessed across VFU tr/ts curve slopes (n=9 experiments). Individual experiments (blue symbols) were averaged to give overall results (large blue circles), and statistical tests were run on both period and standard deviation. Repeated Measures ANOVA indicated that the effect

of slope on period was not significant ($p > 0.05$), but the effect on standard deviation was significant ($p<0.001$). Planned comparisons were used to further test the standard deviation of network period for the m=0 case against the standard deviation at nonzero slopes, as this slope gives a minimum stability criterion, and results indicated that variability at m=0 was less than at all other slopes. Error bars reported as +/-1 S.E. adjusted for repeated measures data (O'Brien and Cousineau, 2014).

For the subset of hybrid networks constructed from a PD without significant autocorrelation in the uncoupled intrinsic cycle periods, we assessed how well the predicted distributions of hybrid network period matched the corresponding distributions of period observed in the hybrid networks across VFU tr/ts curve slopes. Prediction of the mean period of the distribution was highly accurate across VFU slopes, with an average error of 1.69% (Fig. 14A) between predicted and observed values. The average error between the predicted and observed standard deviation of the distributions had an average magnitude of prediction error of 16.63% (Fig. 14B). Most of the observed prediction error for variability in network period appears to be relatively independent of VFU tr/ts curve slope, such that the relationship of variability to slope is accurately predicted. Both the prediction and observation of average network period variability were at a minimum when the slope of the VFU tr/ts curve was zero.

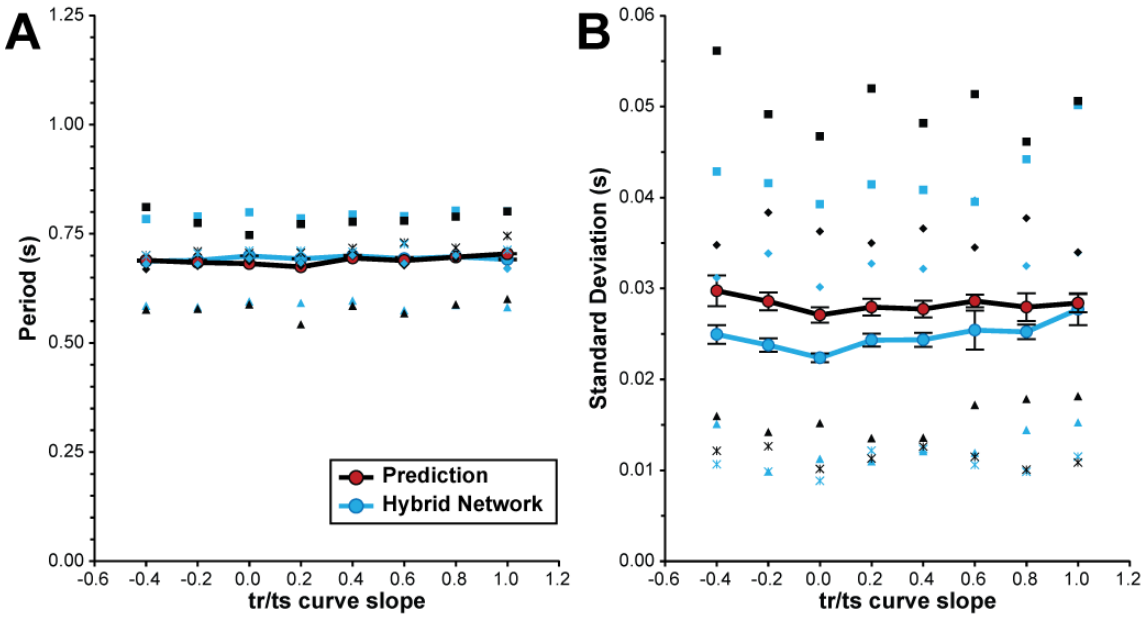

Figure 14. Comparison of predicted to observed network period and variability. Experiments for which predictions and observations of period and variability were made and no strong autocorrelation was present are compared (n=4). Individual measurements of both observed hybrid network activity (blue) and predicted activity (black) were plotted (using the same symbols for results from the same preparation) and averaged (large circles), showing good correspondence between predictions and observed hybrid network activity. Error bars: +/-1 S.E. for repeated measures data.

An analytic solution for a constant recovery interval in VFU

Our theoretical and experimental results indicate that the VFU utilizing a zero slope tr/ts curve produces minimum variability in network period. We examined this special case and obtained a simple analytical solution. If the slope is equal to zero, the recovery interval in the VFU is constant: $tr_{VFU} = g_{VFU}(ts_{VFU}) = tr^*_{VFU}$, and the map would converge to steady-state in one cycle by a single vertical step without need of any horizontal paths in Fig. 9B. Consequently the recovery interval in PD depends only upon the random intrinsic period of PD with no dependence on previous recovery intervals or their distribution $\varrho_{tr_{PD}}(\tau)$. In this case the recovery interval in PD may be represented as a function of one variable: $tr_{PD}[n+1] = g_{PD}(b, P_{PD}[n]) = \overline{g_{PD}}(P_{PD}[n]) =$

$P_{PD}[n]/P_0\ g_{PD}(b\ P_{PD}[n]/P_0)$ and the integral in *Eq. 6* takes a very simple form that can be solved analytically for the distribution $\varrho_{P_{PD}}$ and tr/ts curve $\overline{g_{PD}}(P_{PD}[n])$ by changing variables $p = \overline{g_{PD}}^{-1}(tr_{PD})$ and $dp = \overline{g_{PD}}^{-1\prime}(tr_{PD})\ dtr_{PD}$:

$$\varrho^*_{tr_{PD}}(tr_{PD}) = \int_{\Omega(P_{PD})} \varrho_{P_{PD}}(p)\delta\big(tr_{PD} - \overline{g_{PD}}(p)\big)dp$$

$$= \left|\overline{g_{PD}}^{-1\prime}(tr_{PD})\right|\varrho_{P_{PD}}\left(\overline{g_{PD}}^{-1}(tr_{PD})\right) \qquad (7)$$

Using equation (7) we can find the distribution of PD's periods when it is coupled with the VFU with zero slope.

$$\varrho_{P_{net}}(P_{net}) = \left|\overline{g_{PD}}^{-1\prime}(P_{net} - tr^*_{VFU})\right|\varrho_{P_{PD}}\left(\overline{g_{PD}}^{-1}(P_{net} - tr^*_{VFU})\right) \qquad (8)$$

Eq. 8 is similar to the distribution of periods in a feedforward network with a stochastic element (Tikidji-Hamburyan et al., 2014) and has a simple intuitive explanation. P_{net} is a function of P_{PD}, and there is a simple rule for scaling the probability density of a function of a variable when the probability function of the original variable is known (Larson and Shubert, 1979). *Eq. 8* uses this rule directly to make the area under the curve for $\varrho_{P_{PD}}$ for a given ΔP_{PD} equal to the area under the curve for $\varrho_{P_{net}}$ for a given ΔP_{net} (and shows that for the special case given above, the result agrees with known theory). If (and only if) the tr/ts curve is flat, the recovery interval in LP/VFU is constant, which removes one source of variability by making the stimulus interval in AB/PD constant except for the remaining

source of variability, the stochastic period. This intuitively explains the minimum variability associated with a zero slope.

DISCUSSION

Relevance to pyloric circuit

A recent review (Lamb and Calabrese, 2012) summarized previous work (Nadim et al., 2011) on the role of the LP to PD synapse in stabilizing the AB/PD pacemaker as "overriding the influence of perturbations — either slowing down incipient advances or speeding up incipient delays." In other words, the LP to PD synapse is thought to stabilize the mean value of the network period. In this study, using a combination of experimental and theoretical methods we have extended the role of the LP to PD synaptic feedback to reducing the variability of the network period with dependence upon the tr/ts dynamics of LP, and suggest that the constant rebound response characteristic of the tr/ts dynamics of LP is optimized to minimize variability in the biological pyloric circuit.

The pyloric network has been the focus of much experimental and modeling work that has explored the enticing question of how similar stereotypical rhythmic activity can arise from neurons and networks of neurons with different combinations of underlying properties such as intrinsic membrane conductances and synaptic weights. This non-uniqueness in activity pattern generation is found at the single neuron level (Golowasch and Marder, 1992; Turrigiano et al., 1995; Liu et al., 1998; Prinz et al., 2003a; Taylor et al., 2009), extends through the network level (Prinz et al., 2004b; Grashow et al., 2010; Daur et al., 2012; Gutierrez et al., 2013), and is likely to involve the coordinated regulation of ionic currents and membrane channels (MacLean et al., 2003; Schulz et al.,

2006, 2007; Goaillard et al., 2009; Hudson and Prinz, 2010; Zhao and Golowasch, 2012). A frequently used strategy to evaluate the presence of such non-uniqueness of neuron or network configurations that produce similar functional activity proceeds by first obtaining steady state estimates of the activity characteristics of a given population of neurons or networks, then assessing whether these estimates of activity characteristics conform to some stereotypical pattern or outcome. For biological experiments, this is accomplished by averaging variable network output to obtain estimates of steady state network function. For model data, steady state network activity intervals of simulated activity are typically obtained directly, without averaging, as simulated activity will lack the variability present in a biological neuronal system (Faisal et al., 2008) unless such variability is programmed into the model, which is an uncommon practice. Our results indicate that if insights into how networks are adapted to variability are not integrated into such studies—particularly in modeling studies—it is possible that the examination of steady state output alone may result in false positives when classifying what constitutes a biologically plausible network configuration. In other words, network configurations that are both adapted to produce a stereotypical activity pattern and optimized for variability may be a subset of all network configurations that produce a stereotypical activity pattern.

This point is especially compelling in light of one recent study that has found that relationships can exist between individual cellular conductances and neuronal phase response dynamics (Soofi and Prinz, 2015), which implies that it may be possible to trace the locus of network adaptations for rhythmic variability back to ionic current expression. This insight makes it tempting to speculate, for instance, that a zero slope tr/ts curve in

LP might depend upon a similar association as was shown in another study to occur between animal-to-animal preservation of PD rebound response following inhibition and correlation of the ionic currents transient A-type current I_A and hyperpolarization-activated current I_H (Zhao and Golowasch, 2012). But future studies will be required to address these kinds of questions and may not prove trivial, as ionic current correlations have not always proven intuitive, and at least two studies have demonstrated that there are likely to be other ionic currents involved in a pyloric neuron's rebound interval in addition to I_A and I_H (Taylor et al., 2009; Zhao and Golowasch, 2012).

One further question that remains unanswered is whether the pyloric circuit utilizes variability as a beneficial feature to provide flexibility to some behavioral goal in digestion, as has been suggested for the circuit underlying *Aplysia* feeding (Horn et al., 2004), or if variability in pyloric pattern generation is simply a "good enough" solution that generates sufficiently functional patterned activity with a neuronal network of minimal complexity and associated metabolic cost (Selverston et al., 2000; Hooper, 2004). Addressing this question directly is beyond the scope of this paper, but it is interesting that our results, combined with previous findings, imply that in at least two respects the pyloric circuit is configured in a manner that optimally minimizes rhythmic variability: in terms of both its predominance of synaptic inhibition (Selverston et al., 2000; Sieling et al., 2009) and LP feedback. It may be the case that—because the pyloric rhythm interacts with other CPGs within the stomatogastric nervous system such as the gastric mill rhythm—a pyloric network configuration that confers minimal rhythmic variability is necessary for the circuit to maintain functional integrity in the face of inputs from other networks that operate on differing timescales.

There are likely other intrinsic dynamics of neuronal networks that impact network activity variability, such as might occur due to changes in synaptic feedback burst width. In this study we used a simplified form of feedback to the pacemaker by fixing the duration of the input at a constant value representing the mean burst width observed in the biological LP, but in a future study we plan to explore the implications of this simplification on network activity variability by allowing this burst width to vary.

Alternative approaches

One could simply iterate the map in Equation 2 starting from an arbitrary initial condition to obtain the stationary predicted distribution of recovery intervals, drawing the period from the measures distribution with the appropriate probability on each iteration. That approach is related to the one presented in the paper, but the solution could depend upon initial conditions if there are multiple fixed points (see next section).

An earlier paper (Thounaojam et al., 2014) took the approach of recreating the histogram of the firing intervals by iterating exactly the map described in Equation 2 under two different assumptions. The histogram is an approximation of the stationary probability distribution of the intervals. The first assumption was that the period was drawn from a Gaussian distribution and the second assumption was that the period was a history-dependent random process. For that study, the assumption of history dependence gave much better results because the number and stability of attractors appeared to vary slowly. The neurons in that study were not bursting neurons like the neuron utilized in this study, which may explain why history dependence was critical in that study but not

in ours. The variety of the number and types of fixed points in the tr/ts maps (see next section) may also explain part of the difference.

Many other studies (Sieling et al., 2009; Ermentrout et al., 2011; Thounaojam et al., 2014) assume that the intrinsic period is constant but that noise causes the phase of the oscillation to be decoupled from the elapsed time, such that the stimulus interval ts is no longer a reliable indicator of the actual phase at which a neuron receives an input. In that case, the phase variable acquires a stochastic component that is added to the map at the time an input is received, so that effectively the phase resetting has an additive stochastic component. Adding noise to the phase resetting was effective in (Sieling et al., 2009) but not (Thounaojam et al., 2014). In this study, we can measure the variability in the period, and it is greater than the variability in the observed phase resetting, so we chose to address variability in the intrinsic period instead.

Limitations of the methodology

In the examples that we have presented, each pair of tr/ts curves has a single intersection, and that intersection corresponds to a fixed point associated with an alternating firing pattern, which is slightly different depending upon which tr/ts curve associated with a particular value of the intrinsic period in PD is considered. The fixed point can be considered to "wander" in lockstep with the random variable for the intrinsic period. In our examples, the fixed point is always stable and attracting because the slope of the dark purple curve in Fig. 9B, 9C, and 9D is always greater than the light green curve (Thounaojam et al., 2014), which pushes trajectories back toward the fixed point (Fig. 9B). Rigorously, the assumption of an alternating firing pattern requires that there is an odd number of stable fixed points in the tr/ts map and that the stable fixed points

outnumber the unstable ones, so that the trajectory is never pushed to the ends of the map requiring a phase slip (Thounaojam et al., 2014). However, if phase slips are infrequent this assumption can be violated without degrading the quality of the results.

In the presence of second order resetting, the experimental method we employed to measure the tr/ts curves is not valid. Beyond the fact that second order resetting is not directly measurable using a multiple-pulse PRC protocol, the theoretical methods employed here assume tr/ts curves are equivalent to those constructed from a single-stimulus PRC protocol. With second order resetting the map methods become much more complicated (Oprisan and Canavier, 2001).

Another limitation of the theoretical method is that in its present form, it only strictly applies to intrinsic oscillators whose intrinsic period has no history dependence. Only half of the experimental preparations met this criterion for analysis by our theoretical methods. We have devised a map that takes into account the history dependence of the period (Thounaojam et al., 2014). An extension of the theory presented herein to that case remains to be done. Several preparations show such history dependence (Netoff et al., 2005; Deister et al., 2013; Thounaojam et al., 2014). This history dependence has been hypothesized to play a role in active decorrelation in the basal ganglia (Wilson, 2013), so such an extension may have broad applicability.

One source of history dependence is gastric modulation (Clemens et al., 1998; Bucher et al., 2006). We have not proved that a zero slope of the LP tr/ts curve decreases variability in the presence of sources of history dependence like gastric modulation, but it seems likely that removing a source of variability in this manner would tend to decrease the total variability under any circumstances.

Relevance to general theory of central pattern generation

To our knowledge this is the first study to have examined a biological neuronal network system to assess the role of the intrinsic phase dynamics of its feedback neurons towards regularity in rhythm generation. Due to the relatively recent discovery that tr/ts techniques can be extended to analyze the phase response dynamics of rhythmic networks that include non-endogenously bursting neurons, it is not yet known how many other pattern generating systems tend to be optimized in this way for regularity like the pyloric network. Further studies can elucidate this.

The methods presented in this paper are general and can be applied to two oscillators or two PIR elements, in addition to a circuit with one oscillator and one PIR element as presented herein. In our study, matching the particular shape of the distribution of intrinsic periods was important in order to obtain a good match to the data. However, the qualitative effect on the width of the distribution of any feedback strategy can be determined by calculating its effect on a Gaussian distribution, for example. This allows the determination of optimal feedback strategies for other central pattern generators driven by an intrinsically bursting kernel, for example the mammalian respiratory central pattern generator (Marder and Bucher, 2001).

CHAPTER 3: CYCLE TO CYCLE BURST WIDTH TIMING IN A CENTRAL PATTERN GENERATOR AND CYCLE PERIOD VARIABILITY

INTRODUCTION

Central pattern generators underlie repetitive motor pattern expression, and study of these systems has taught us much about seemingly disparate questions about network reliability and variability, how stereotypical network activity arises from the interplay of underlying neuron and synapse properties, and how stereotypical activity patterns are preserved in the face of changes to the network. The pyloric network of the decapod crustacean is a central pattern generator that has been studied in all of these contexts, so is well suited for formulating questions by integrating previous findings into new insights. Here we consider and attempt to integrate two threads of research in the pyloric network: first, that network feedback to a pyloric central pattern generator has been shown to stabilize network period and do so optimally based upon at least two inherent features of their network configuration (Selverston et al., 2000; Sieling et al., 2009; Nadim et al., 2011; Hooper et al., 2015); and second, that pyloric network activity has also been shown to undergo phase maintenance under a variety of changes imposed on a network, such as altered injection current and temperature, both in vitro and in vivo (Hooper, 1997a, 1997b; Katz et al., 2004; Tang et al., 2010; Soofi et al., 2014). In particular, what has not yet been studied to our knowledge is how rapidly or slowly this phase maintenance occurs. If phase maintenance is rapid, a natural question follows: could it play a role in stabilizing the pyloric network? Because recent work has

demonstrated that biological pyloric network configuration optimally minimizes rhythmic period variability in two studied features of network composition: the predominance of inhibitory synapses (Selverston et al., 2000; Sieling et al., 2009) and the phase response dynamics of synaptic feedback to the pacemaker (Hooper et al., 2015), any systematic patterns of burst width regulation would seem likely candidates for playing a similar role. These are the questions we will attempt to address in this study.

The pyloric network's activity consists of a stereotyped triphasic bursting pattern driven by the anterior burster/pyloric dilator (AB/PD) pacemaker complex (Russell and Hartline, 1978; Bal et al., 1988; Harris-Warrick and Marder, 1991), which itself consists of an electrically coupled group of one AB neuron and two PD neurons, all of which burst in synchrony and produce the first phase of the rhythm (Fig. 15B,C,D in green). The AB/PD projects inhibitory synapses to two follower neuron groups within the pyloric network (fig. 15C, synapses with open circles are cholinergic, synapses with filled circles are glutamatergic). The target neurons of these projections are the lateral pyloric neuron (LP, one per STG) and the pyloric neurons (PY, 5-6 each per STG). Functionally these follower neurons are distinguished by their participation in bursting network oscillation via post-inhibitory rebound, meaning that they fire bursts following the application and removal of inhibitory synaptic input. In this way LP and PY are conditional bursters at the pyloric network's oscillation frequency, and absent synaptic inhibition are either silent or spike tonically (Fig. 15D).

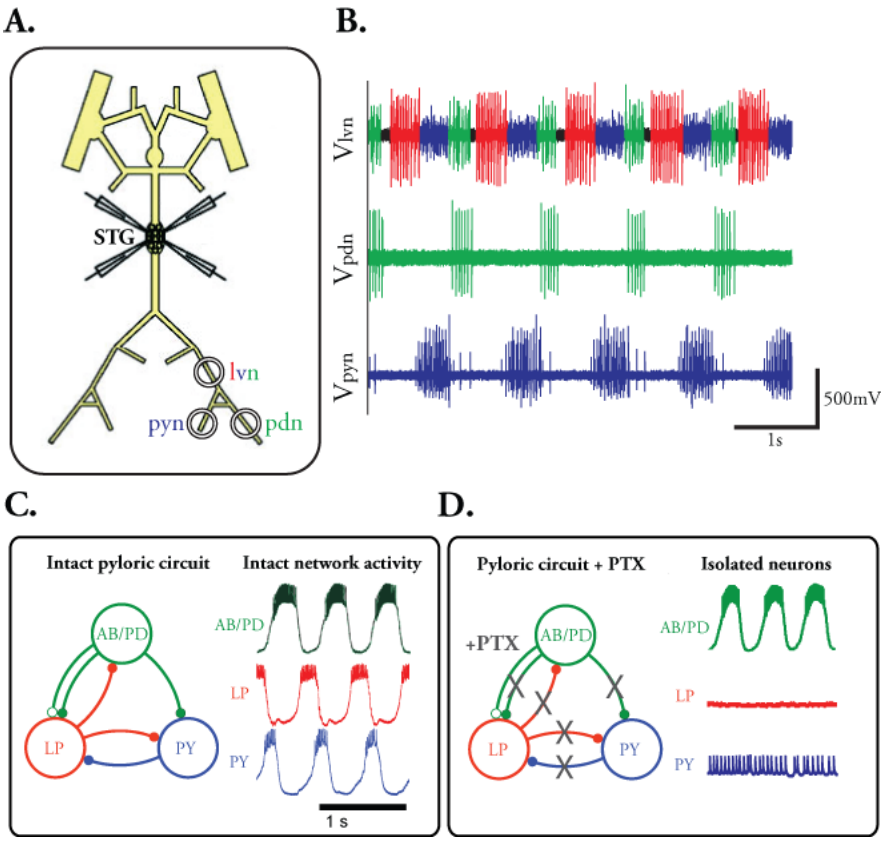

Figure 15. Crustacean STNS (A). The Stomatogastric Ganglion (STG) contains the somata of the pyloric network, while extracellular recordings can be taken from the motor nerves: lateroventricular nerve (lvn, contains motor nerves for LP [red], PY [blue], and PD[green]), and the nerves of PY and PD (pyn and pdn). Adapted from Marder and Bucher, 2007. Recorded extracellular traces displaying triphasic rhythm on lvn (B). The intact network pyloric network (C) generates a triphasic bursting rhythm by utilizing a pacemaker neuron group (AB/PD), which leads the rhythm, and two types of follower neurons (LP and PY) that burst in response to post-inhibitory rebound imposed by synaptic input from AB/PD. Reciprocal inhibition between LP and PY and synaptic feedback from LP to PY, as well as the presence of synaptic depression, are important features of this circuit. Bath application of PTX (D) pharmacologically blocks glutamatergic synapses in the pyloric network, which has the effect of synaptically isolating AB/PD, and minimizing synaptic inhibition of the follower neurons. The resulting network activity reveals the intrinsic rhythmicity of AB/PD along with the lack of propensity of LP or PY to burst on their own on a pyloric timescale.

Following exploration of the pyloric network's cycle by cycle phase maintenance properties, we use insights gained to inform three hybrid network configurations constructed using the dynamic clamp. The first two strategies were based upon

observations of the intact pyloric network (see Results), while the third was a theoretical strategy chosen because it was mathematically complementary to the experimentally inspired strategies.

METHODS

General experimental methods

Adult *C. Borealis* crabs were obtained via overnight shipping from The Fresh Lobster Company (Gloucester, MA) and maintained in artificial seawater at 10°C. Crabs were anesthetized in ice for 30 minutes prior to dissection. The STG was dissected as described previously (Gutierrez and Grashow, 2009) and pinned out in a Sylgard lined dish containing chilled physiological saline (in mM: 440 NaCl, 11 KCl, 13 $CaCl_2$, 26 MgCl2, 12.4 Trizma base, 5.3 Maleic acid, pH 7.45 @ 13°C). The STG was desheathed and Vaseline wells were formed around the lateral ventricular nerves. All preparations were perfused with physiological saline maintained at 12-14°C. All electrophysiological data were digitized on a Digidata 1322A (Axon Instruments) with an 84μs sampling interval and recorded using Clampex 9 software (Axon Instruments). Extracellular recordings were made from the wells using stainless steel electrodes inserted into the Sylgard, and signals were filtered and amplified by an A-M Systems Model 1800. Intracellular recordings were made with an Axoclamp 2B amplifier (Axon Instruments) in discontinuous current-clamp mode using glass microelectrodes (10-20 MΩ) filled with a solution of 0.6 M K_2SO_4 and 20 mM KCl. PD neurons were identified with standard procedures for *C. borealis* (Selverston and Moulins, 1976; Harris-Warrick, 1992) then pharmacologically isolated from glutamatergic synaptic input from LP using

physiological saline containing 10^{-5} M Picrotoxin (PTX, Sigma-Aldrich) (Bidaut, 1980). Dynamic clamp (Dorval et al., 2001) protocols were programmed in house and run with an update rate of 50 μs on a computer with a NI PCI-6052E data acquisition card (National Instruments). In all dynamic clamp protocols, burst onset of rhythmic biological membrane voltage traces is defined as occurring when the rising phase of the slow oscillation crosses a voltage threshold. This threshold was chosen to fall where the rising phase of the slow oscillation was steepest in order to ensure maximum tolerance to baseline drift, and the slow oscillation trace was isolated from spikes by filtering the membrane voltage trace according to $V_{filt}(t + \Delta t) = V_{filt}(t) + [V_m(t + \Delta t) - V_{filt}(t)]\Delta t/\tau_{filt}$, where V_{filt} is the filtered membrane voltage, V_m is the unfiltered membrane voltage, Δt is the dynamic clamp time step of 50 μs , and τ_{filt} = 50 ms. Analysis of all recordings was performed offline in Spike2 (Cambridge Electronic Design).

Hybrid networks

Using the dynamic clamp and pharmacologically isolated biological PDs from N=12 experimental preparations, we constructed hybrid network in each preparation that approximate intact pyloric network activity (Fig. 16A) using three different forms of a virtual feedback unit (VFU) model representing LP (Hooper et al., 2015), randomizing presentation order of these forms across preparations. Briefly, a VFU model is designed to simulate LP synaptic feedback to PD (Fig. 16B) by representing the synaptic input simply as a square conductance pulse of duration B_{VFU} that occurs at a response interval tr_{VFU} following the last received synaptic input from PD (Fig. 16D). In general, the

response interval tr is a function of the stimulus interval ts—the interval between a neuron's previous burst and the receipt of synaptic input (Fig. 16D). This tr/ts relation is a generalized extension of phase response analysis that can be applied to neurons with non-endogenous oscillations of the LP (Sieling et al., 2012), in addition to being applicable to neurons with the endogenous oscillation required by conventional phase response theory (Ermentrout, 1996; Schultheiss et al., 2012). But because our previous work has shown that tr is independent of ts in LP, here all VFUs utilized a constant response interval tr^*_{VFU} based upon intact LP activity, i.e. a tr/ts curve with slope zero (Fig. 16C). This fixed response interval reproduces the response interval of LP scaled to account for any change in period between intact network activity measurement and hybrid network formation, such that $tr^*_{VFU} = P_0 \cdot \overline{\Phi r}_{LP}$, where the mean period of PD just prior to hybrid network formation P_0 is used as an estimate of the hybrid network period P_{HYB}, and $\overline{\Phi r}_{LP}$ is the mean response phase of LP in the intact pyloric network $\overline{\Phi r}_{LP} = \bar{t}\bar{r}_{LP}/P_{INT}$. All interval means were assessed over 40 cycles.

Instead of synaptic input from PD being mediated by actual or simulated synaptic current as a biological or model neuron would, respectively, a VFU estimates the onset of received synaptic input as coincident with burst onset of PD, defined as dynamic clamp detection of threshold crossing in PD's membrane voltage. Other aspects of the PD to LP synapse such as synaptic strength and synaptic input duration are implicitly accounted for by the VFU, since the VFU is designed to respond to PD input with timing identical to that of LP's response to PD.

The VFU to biological PD artificial synapse consisted of a 50nS virtual conductance with instantaneous activation and a reversal potential of -90mV. Both

selected values of conductance and reversal potential were based upon previous voltage clamp measurements from this synapse (Thirumalai, 2002; Archila and Prinz, 2012; Archila, 2013).

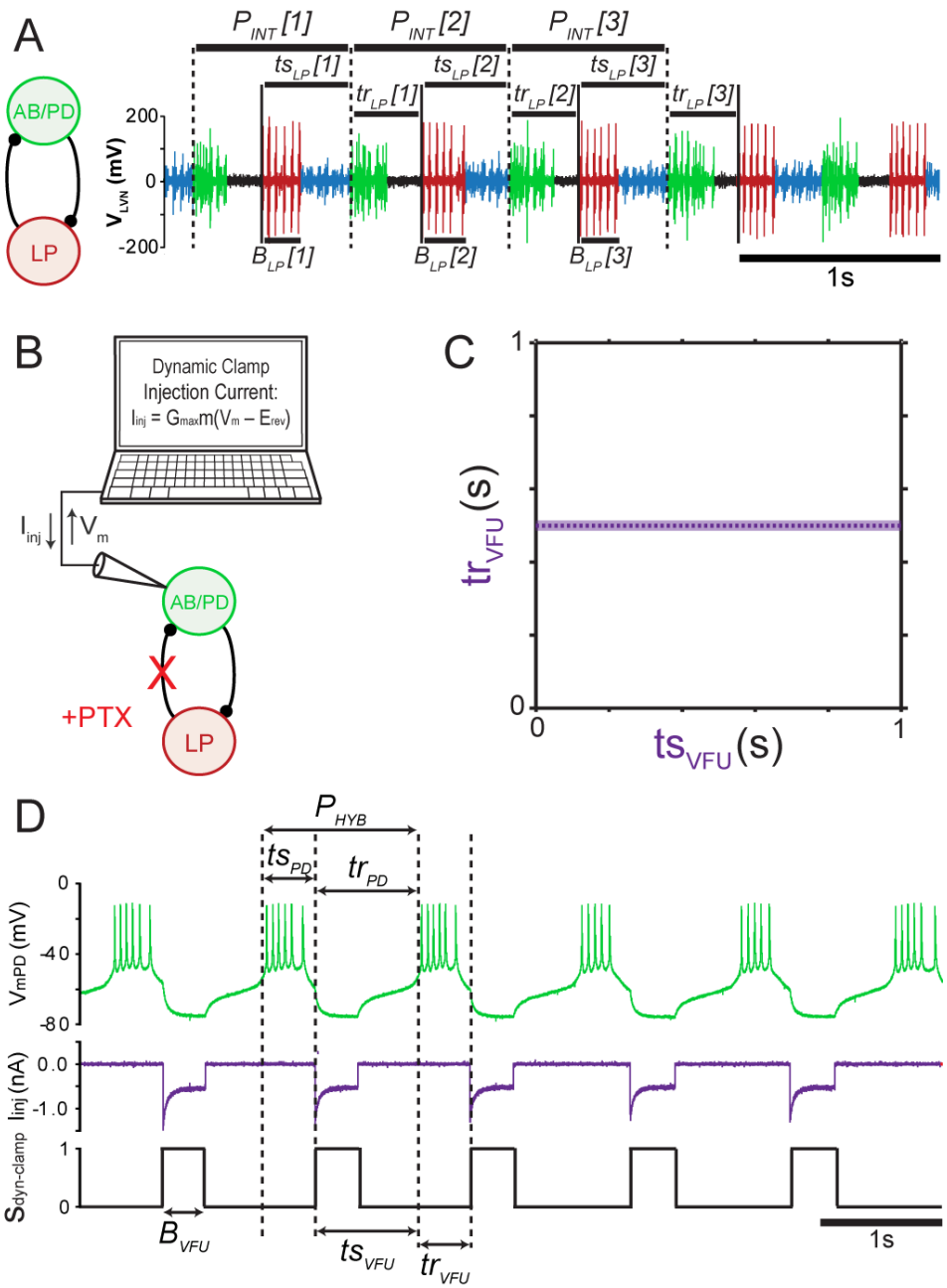

Figure 16. Virtual Feedback Unit (VFU) models of LP are (A) based upon LP's activity intervals tr_{LP} and ts_{LP} measured from extracellular recordings of intact pyloric network prior to pharmacological dissection of the network. Corresponding intact network periods (P_{INT}) are measured between first spikes of bursts in PD. Using the dynamic clamp to inject artificial conductance in PD, the feedback role of LP is reprised by the VFU by

directly reproducing equivalent timing of intervals measured in LP, including (C) tr/ts relationship and (D) burst duration B_{VFU}.

VFU burst width regulation strategies

In each preparation we implemented three different forms of hybrid network distinguished by their feedback equation governing VFU burst width B_{VFU} (Fig. 16D). Our first synaptic feedback strategy is implemented as a VFU with fixed duration feedback burst B_{VFU} (figure 17A), represented by the recurrence:

$$B_{VFU}[n+1] = B_{VFU}[n] = \hat{B}_{LP} = \overline{DC}_{LP} \cdot P_0 \qquad (1)$$

where the equality of B_{VFU} as the index is iterated indicates that the quantity is independent of network cycle n. The fixed value $\hat{B}_{LP}$ is the burst duration of the biological LP, scaled to account for any change in period between intact pyloric network activity measurement and hybrid network formation, and is determined using both the mean duty cycle of LP's burst width in the intact pyloric network $\overline{DC}_{LP} = \bar{B}_{LP}/P_{INT}$, and the mean period of the isolated PD just prior to establishing the hybrid network P_0.

Our next synaptic feedback strategy scales VFU burst width proportionally with spontaneous changes in network period on a cycle-by-cycle basis. We refer to this as a directly proportional burst regulation strategy (figure 17B). Because of causality VFU burst width is calculated by scaling the LP duty cycle by the preceding network period, according to the recurrence:

$$B_{VFU}[n+1] = \overline{DC}_{LP} \cdot P_{HYB}[n] \qquad (2)$$

Our third strategy performs the inverse of the directly proportional DC burst, which we term the inversely proportional burst regulation strategy (figure 17C). It is calculated as follows:

$$B_{VFU}[n+1] = (\overline{DC}_{LP} \cdot P_0)\, P_0/P_{HYB}[n] = \hat{B}_{LP} P_0/P_{HYB}[n] \qquad (3)$$

Note that for all three VFU burst regulation strategies, a spontaneous network cycle period $P_{HYB} = P_0$ results in the generation of a VFU burst width $\hat{B}_{LP}$, which will also be the mean VFU burst generated in the absence of any slow drift in period.

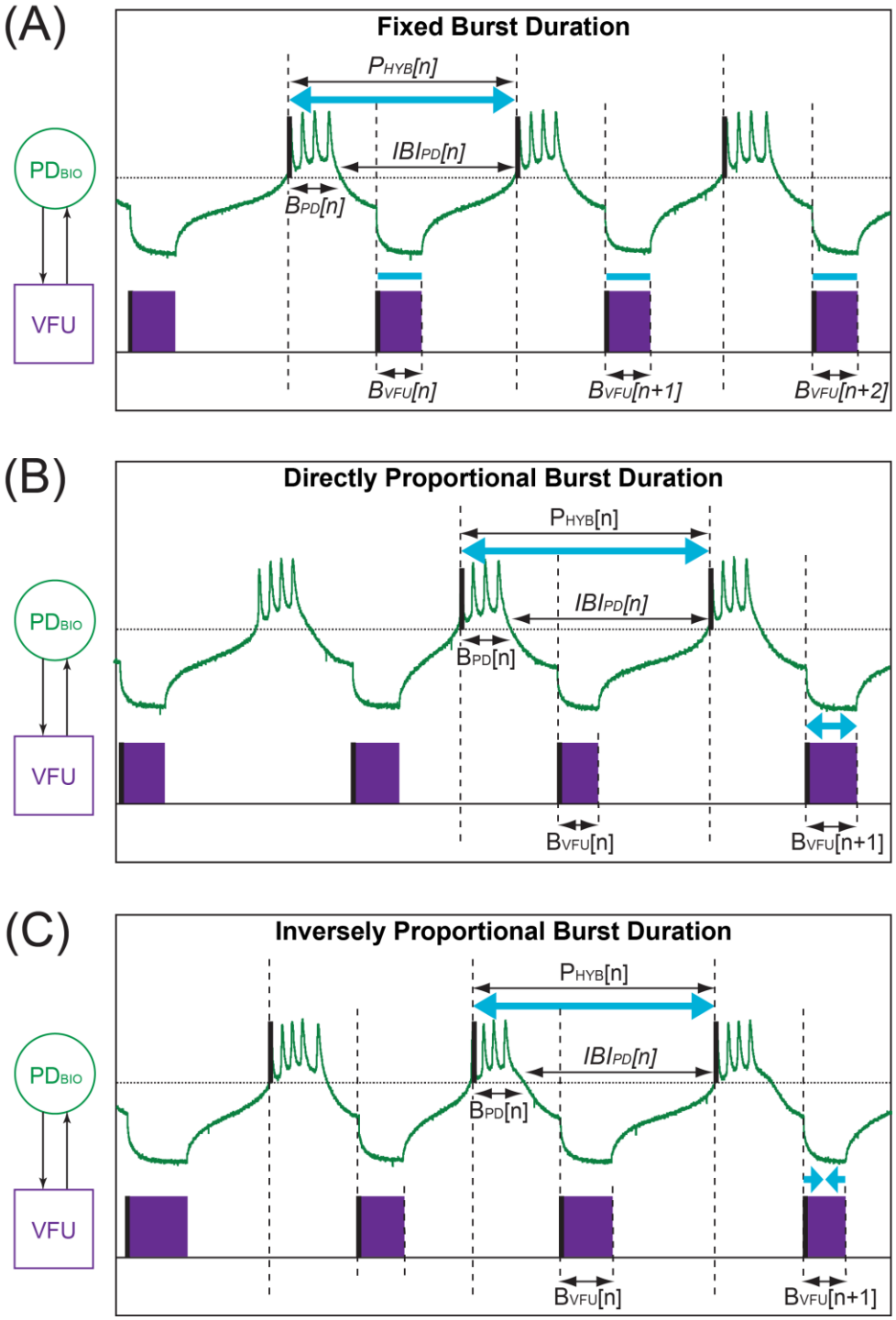

Figure 17. Inhibitory synaptic feedback burst width strategies: (A) fixed burst duration (eqn. 6), (B) directly proportional burst duration (eqn. 7), (C) inversely proportional burst duration (eqn. 8). Heavy blue arrowed bars above hybrid network period P_{HYB} show spontaneous increases in period, while corresponding heavy blue arrowed bars above VFU bursts show resulting changes in VFU burst width B_{VFU} due to regulation strategy. Hybrid network activity intervals that changes in B_{VFU} may impact are illustrated above as period P_{HYB}, network PD burst width B_{PD}, and network PD interburst-interval IBI_{PD}.

Statistical Analysis

Statistical relationships between pyloric network period and LP burst width were assessed in N=20 intact pyloric preparations using the statistics and signal processing toolboxes in MATLAB. Correlation was calculated on sequences of 50 consecutive cycles as Pearson's correlation coefficient *r* with corresponding p-values calculated assuming a two-tailed t-distribution. Following standardization of the same sequences, cross-correlation functions were calculated for 20 lags in each direction for a total of 41 lags (including zero lag) and normalized. Autocorrelation functions of each sequence's pyloric network period were then calculated using 20 lags. 95% confidence intervals were estimated in the standard manner as $\pm 1.96/\sqrt{n}$, where n is the number of cycle periods in each sequence. Optimal predictors for LP burst width were constructed using combinations of lagged pyloric network periods and optimized to maximize correlation of the predictor to LP burst width using unconstrained nonlinear optimization.

Inferential statistics on hybrid network activity was performed using the analytics software package SPSS 21 (IBM). Required sample sizes were calculated *a priori* using GPower 3.1 (Faul et al., 2007) and four initial datasets, which were included in the final analysis. In all statistical tests the same hybrid network activity features (period P_{HYB}, network PD burst width B_{PD}, network PD interburst-interval $IBI_{PD} = P_{HYB} - B_{PD,}$ and standard deviation (SD) of each) were measured under all conditions of VFU burst width regulation strategy from the same experimental preparation and accordingly treated as repeated measures data for analysis. One-way repeated measures analysis of variance (rANOVA) was performed for each hybrid network activity feature, and if an effect was found to be present, Bonferroni corrected pairwise comparisons were made between VFU

burst width regulation strategies (Maxwell, 1980). Standard errors were calculated with correction for repeated measures designs (O'Brien and Cousineau, 2014).

RESULTS

Cycle-by-cycle LP burst regulation in the intact pyloric network

The pyloric network has been long known to exhibit phase maintenance of activity intervals such as LP burst duration with imposed changes in network period (Hooper, 1997a, 1997b; Katz et al., 2004; Tang et al., 2010; Soofi et al., 2014), meaning that activity intervals such as LP burst width scale with broad changes imposed on network period. But much less is known of the relationship between period and burst duration during ongoing, spontaneous variation in network period. To examine the extent to which phase maintenance is a factor in more rapid transitions in network activity, i.e. in activity fluctuations on a cycle-by-cycle basis, we measured activity from N=20 intact pyloric networks and examined data for intact pyloric network period P_{INT} and LP burst width B_{LP}. Among these preparations, most (15/20 = 75%) experienced statistically significant phase maintenance of B_{LP} as assessed by correlation analysis (Fig. 18A1,A2,B1,B2). These preparations further exhibited large, statistically significant peaks in their cross-correlation function at lag 0 (Fig. 18A5,B5), indicating that network period and LP burst width are strongly correlated within individual cycles. This can be seen in coordinated fluctuations of standardized values for P_{INT} and B_{LP} in plots of successive activity intervals (Fig. 18A3). This large peak in cross-correlation at lag 0 was observed both in preparations without autocorrelation (Fig. 18A3-5, 8/20 = 40% of

preparations), as well as in preparations that exhibited autocorrelation of network period (Fig. 18B-5, 7/20 = 35% of preparations).

The remaining preparations (5/20 = 25%, Fig. 18C) exhibited no cycle-by-cycle regulation of burst width in terms of either overall correlation (Fig. 18C1,2) or cross-correlation (Fig. 18C5), while expressing no significant autocorrelation in network period (Fig. 18C4). No hybrid networks were observed with significant autocorrelation and fixed B_{LP}.

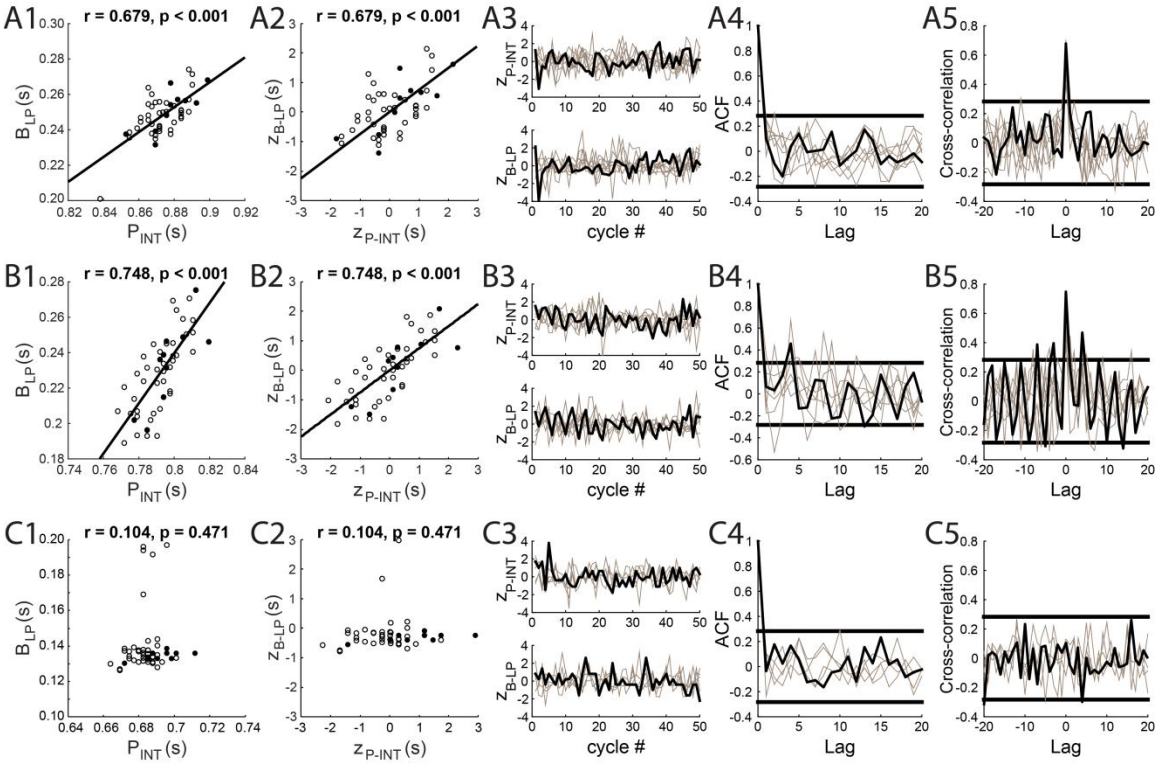

Figure 18. Statistical relationship between intact pyloric network period P_{INT} and LP burst width B_{LP}, assessed in N=20 preparations. Most observed networks exhibited (A1) phase maintenance with a statistically significant positive Pearson's correlation coefficient r between P_{INT} and B_{LP} over n=50 consecutive network cycles, which is also evident when (A2) P_{INT} and B_{LP} are plotted against each other after converting to their standardized values $z_{P\text{-}INT}$ and $z_{B\text{-}LP}$. (A3) Plots of the progression of $z_{P\text{-}INT}$ and $z_{B\text{-}LP}$ indicate that changes in P_{INT} are closely matched by changes in B_{LP} in the same cycle. In (A4) preparations that exhibit both phase maintenance and no autocorrelation (8/20 =

40%), (A5) the apparent cycle-by-cycle phase maintenance of A3 is revealed to be statistically significant by a single positive peak at lag 0 of the cross-correlation function. (B1-B5) Preparations observed to exhibit significant autocorrelation (7/20 = 35%) appeared to exhibit phase maintenance and possess strong peaks a zero-lag, similar to preparations in A1-A5. (C1-C5) Some preparations (5/20 = 25%) exhibited no phase maintenance such that B_{LP} remained relatively fixed independent of P_{INT}.

To estimate how many cycles are of intact pyloric network activity are of primary importance in describing the observed relationship between P_{INT} and B_{LP} in preparations that exhibited significant cross-correlation, we constructed three predictors of each sequence $B_{LP}[n]$ based upon linear combinations of one, two, or three sequential network periods. The first predictor θ_0 was simply set to the intrinsic network periods containing concurrent LP bursts being predicted, such that,

$$\theta_0 = P_{INT}[n] \tag{4}$$

Two additional predictors θ_1 and θ_2 were constructed using linear combinations of multiple periods, such that,

$$\theta_1 = \beta_0 P_{INT}[n] + \beta_1 P_{INT}[n-1] \tag{5}$$

$$\theta_2 = \beta_0 P_{INT}[n] + \beta_1 P_{INT}[n-1] + \beta_2 P_{INT}[n-2] \tag{6}$$

where parameters β were optimized to yield maximum correlation of the predictor with $B_{LP}[n]$ (see *Methods*). These predictor sequences were then correlated with $B_{LP}[n]$ (Fig. 19A), which revealed that the addition of more than one period term to the predictor only yielded a marginal increase in correlation to B_{LP} in all but one preparation. This result combined with a lack of consistent sign for any of the added parameters beyond β_0 (Fig.

19B) indicates that across preparations, feedback burst width regulation is most strongly and consistently understood as being correlated with a single network cycle period.

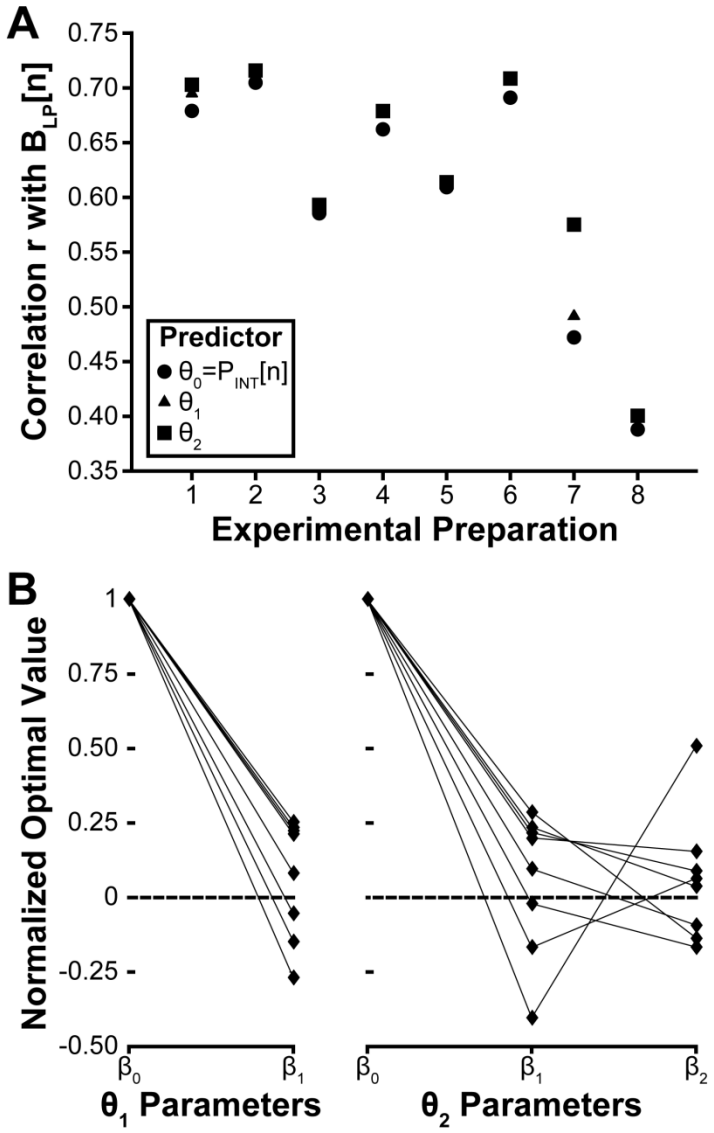

Figure 19. Comparison of correlations of optimal network attribute predictors to LP burst width (B_{LP}) and corresponding parameters of the predictors show that the intact pyloric network's B_{LP} is strongly proportional to a single network cycle period. (A) Three predictors θ_0, θ_1, and θ_2 that utilize combinations of either one, two, or three intact network periods (P_{INT}), respectively, are tested for their correlation with B_{LP} in N=8 experimental preparations. In all but one preparation (preparation n=7) the use of additional preceding cycle periods in the predictor results in only marginal increase in correlation with B_{LP}. (B) Optimized parameters of the predictors θ_1 and θ_2 are found

using unconstrained optimization to maximize correlation of the predictor with B_{LP}. There are no strong relationships between these parameters across preparations.

Based upon these results, we formulated hybrid networks in N = 12 preparations. In each preparation we connected an pharmacologically isolated AB/PD with a dynamic clamp implemented VFU of one of three strategies implemented to set burst width in each cycle: fixed burst duration, directly proportional burst duration, and inversely proportional burst duration (see *Methods*). The fixed burst duration strategy kept VFU burst duration fixed at a value based upon the intact network's LP burst width. The directly proportional burst width strategy scaled VFU burst width proportionally with measured changes in hybrid network period, which is apparent by observing measured intervals of hybrid network period and VFU burst width (Fig. 20). Given an accurate estimate of P_{HYB}, these VFUs tend to generate average burst duration equal to that of the fixed burst duration VFU implemented in the same preparation.

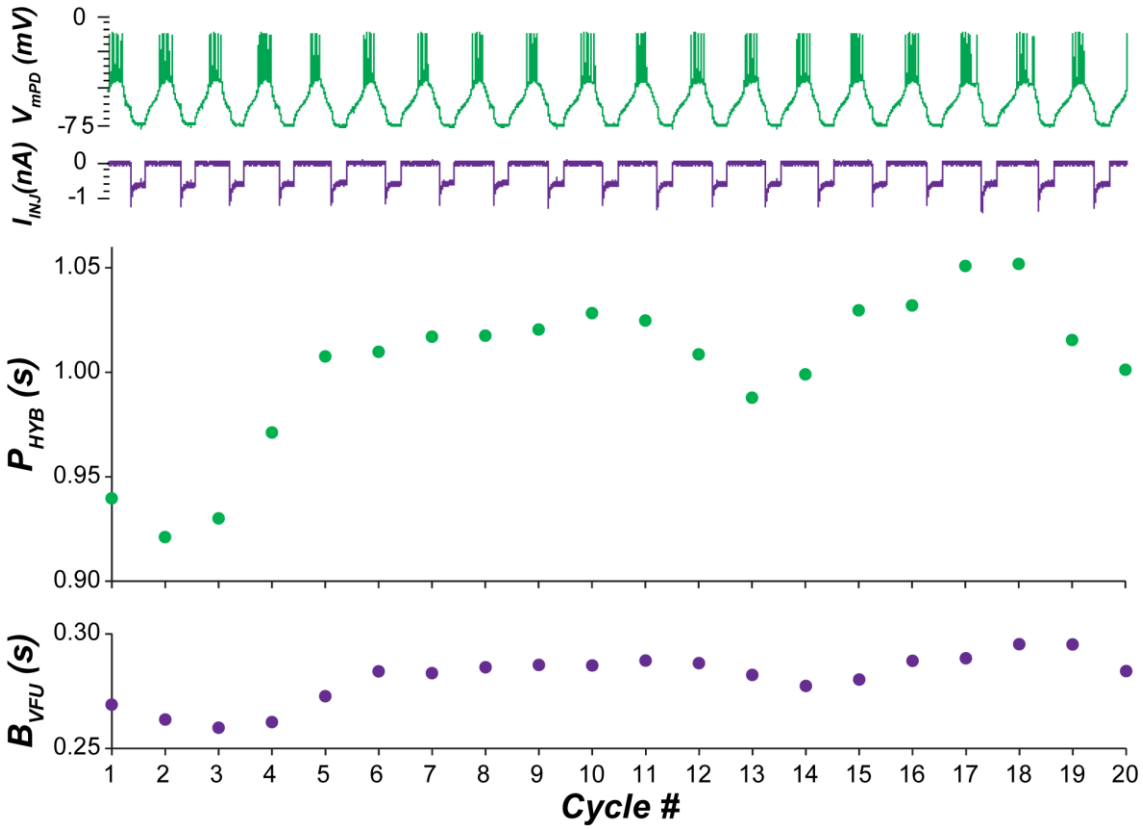

Figure 20. Hybrid network implementation of an AB/PD coupled to a VFU with a directly proportional burst width strategy, with design inspired by observed cycle by cycle phase maintenance in intact pyloric networks. The dynamic clamp implemented VFU burst width B_{VFU} is chosen to be the same fraction of the preceding network period as mean LP burst width was of the mean intact pyloric network period. This hybrid network exhibited autocorrelation (or memory) in its period P_{HYB}, as characterized by the slow drifts in period lasting longer than one cycle, and illustrates the directly proportional changes of B_{VFU} (bottom) with spontaneous changes in P_{HYB}.

Finally, in the same preparations we implemented VFUs utilizing an inversely proportional burst width strategy, formulated to implement anti-phase maintenance on a cycle by cycle basis. Implementation of this strategy in the same preparation as Fig. 20 created networks that exhibited VFU burst width B_{VFU} changes opposite in sign of those observed in network period P_{HYB} (Fig. 21).

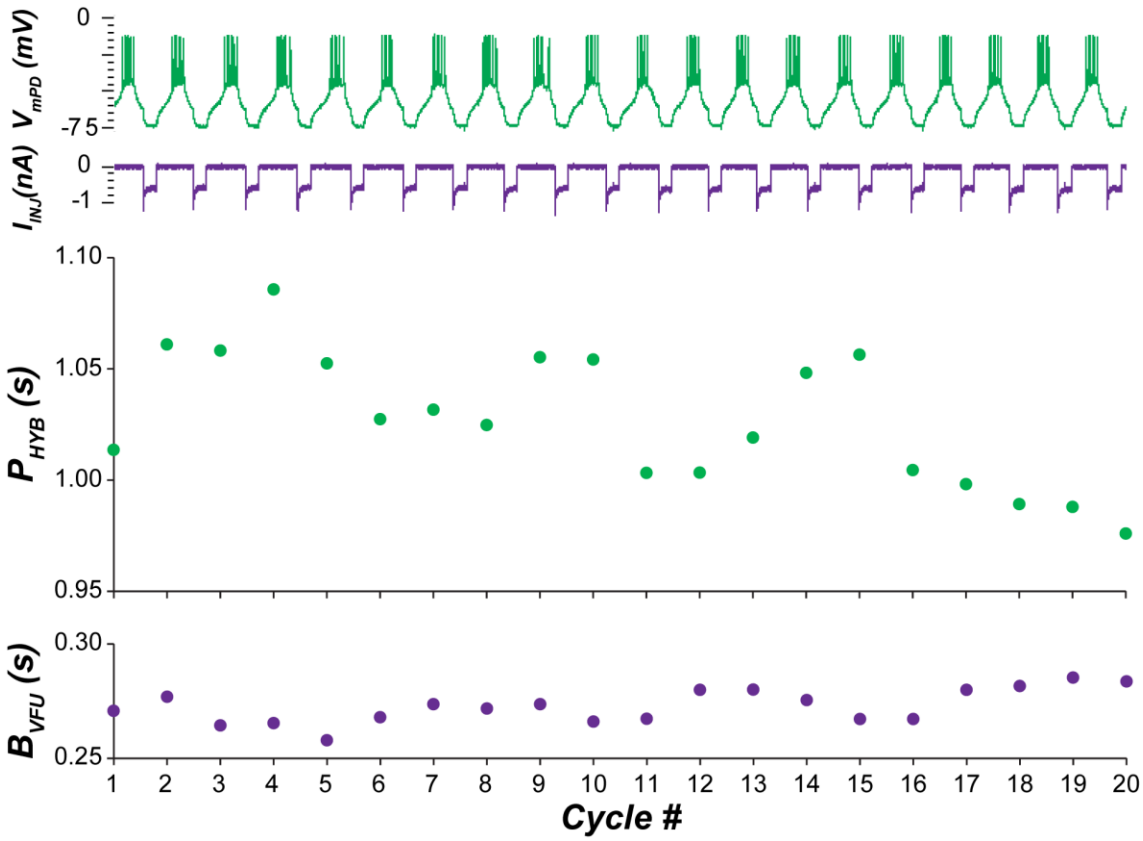

Figure 21. Hybrid network implementation of a AB/PD coupled to a VFU with a inversely proportional burst width strategy. With this strategy B_{VFU} changes occur opposite to those of the directly proportional strategy of Fig. 5, but are designed to be delivered with the same mean value.

Test of mean activity intervals in hybrid networks

Next we wanted to determine if type of burst width feedback strategy had an effect on network period variability, but first we verified that the construction of our different VFU feedback strategies did not yield statistically different mean hybrid network activity intervals as measured by: hybrid network period P_{HYB}, network PD interburst-interval IBI_{PD}, and network PD burst width B_{PD} (see Fig. 20). Any substantial differences in these measures could confound our comparison of variability of these same measures. Separate statistical analyses for each interval across VFU burst width strategies

and preparations as a repeated measures analysis of variance (rANOVA) indicated that there was no statistically significant difference in mean B_{VFU} delivered by each burst width strategy $F(2,22) = 0.079$, $p = 0.924$, as illustrated by plotting the individual experiment means (Fig. 22A1) as well as the grand means each strategy across preparations (Fig. 22B1). Any small differences in B_{VFU} across strategies are due to either nonstationary oscillation period or estimation error of the hybrid network period. There was also no statistically significant effect on hybrid network period P_{HYB} observed with $F(2,22) = 1.548$, $p = 0.235$, as illustrated by plotting the individual experiment means of each VFU burst width strategy in each experiment (Fig. 22B1) as well as the grand means for all experiments (Fig. 22B2). Likewise there was no statistically significant effect of VFU burst width strategy employed on IBI_{PD} as assessed by rANOVA, $F(2,22) = 0.846$, $p = 0.442$ (Fig. 21C), or B_{PD} with $F(2,22) = 0.095$, $p = 0.910$ (Fig. 22D).

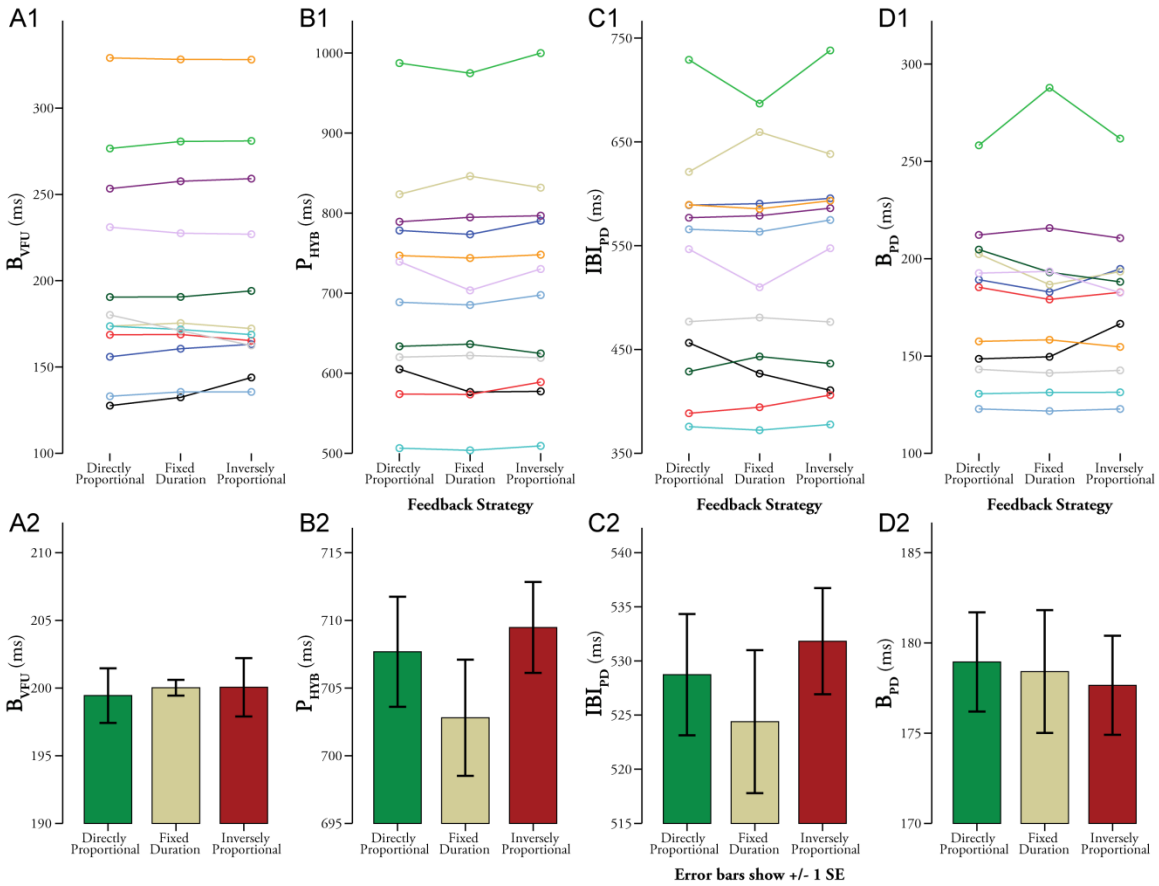

Figure 22. Statistical analysis of hybrid network activity intervals B_{VFU}, P_{HYB}, IBI_{PD}, and B_{PD}. We found no statistically significant differences using rANOVA across VFU burst width strategy employed for VFU burst width B_{VFU} (A), hybrid network PD period P_{HYB} (B), network PD interburst-interval IBI_{PD} (C), and network PD burst width B_{PD} (D). Top subpanels (1) show mean values of each measure observed for each VFU burst width strategy in each individual experimental preparation, while bottom subpanels (2) show grand means across all experiments. Error bars represent SE adjusted for repeated measures data.

Test of variability in hybrid networks

We then examined variability of the same activity measures in our hybrid networks (quantified as standard deviation σ) to determine if network variability depends upon VFU burst width strategy. Beginning with the variability of hybrid network period $\sigma_{P\text{-}HYB}$, using rANOVA we found that there was a statistically significant main effect of VFU burst width strategy, $F(2,22) = 11.23$, $p < 0.001$ (Fig. 23A). Bonferroni corrected

two-tailed pairwise comparisons found that the directly proportional VFU burst width strategy resulted in significantly lower variability in P_{HYB} than in each of the other two burst width strategies. Specifically, a comparison of the directly proportional strategy mean period variability to the fixed duration strategy mean period variability was significant with t(11) = -3.37, p = 0.02; a comparison of the directly proportional strategy mean period variability to the inversely proportional strategy mean period variability was significant with t(11) = -4.16, p = 0.005; and a comparison of fixed duration strategy mean period variability to the inversely proportional strategy mean period variability was not significant with t(11) = -1.97, p = 0.22.

Other measures of activity variability were not significantly different, for network PD interburst-interval variability $\sigma_{IBI\text{-}PD}$ with F(2,22) = 3.27, p = 0.057 (Fig. 23B), and for network PD burst width variability $\sigma_{B\text{-}PD}$ with (F2,22) = 0.24, p = 0.79 (Fig. 23C).

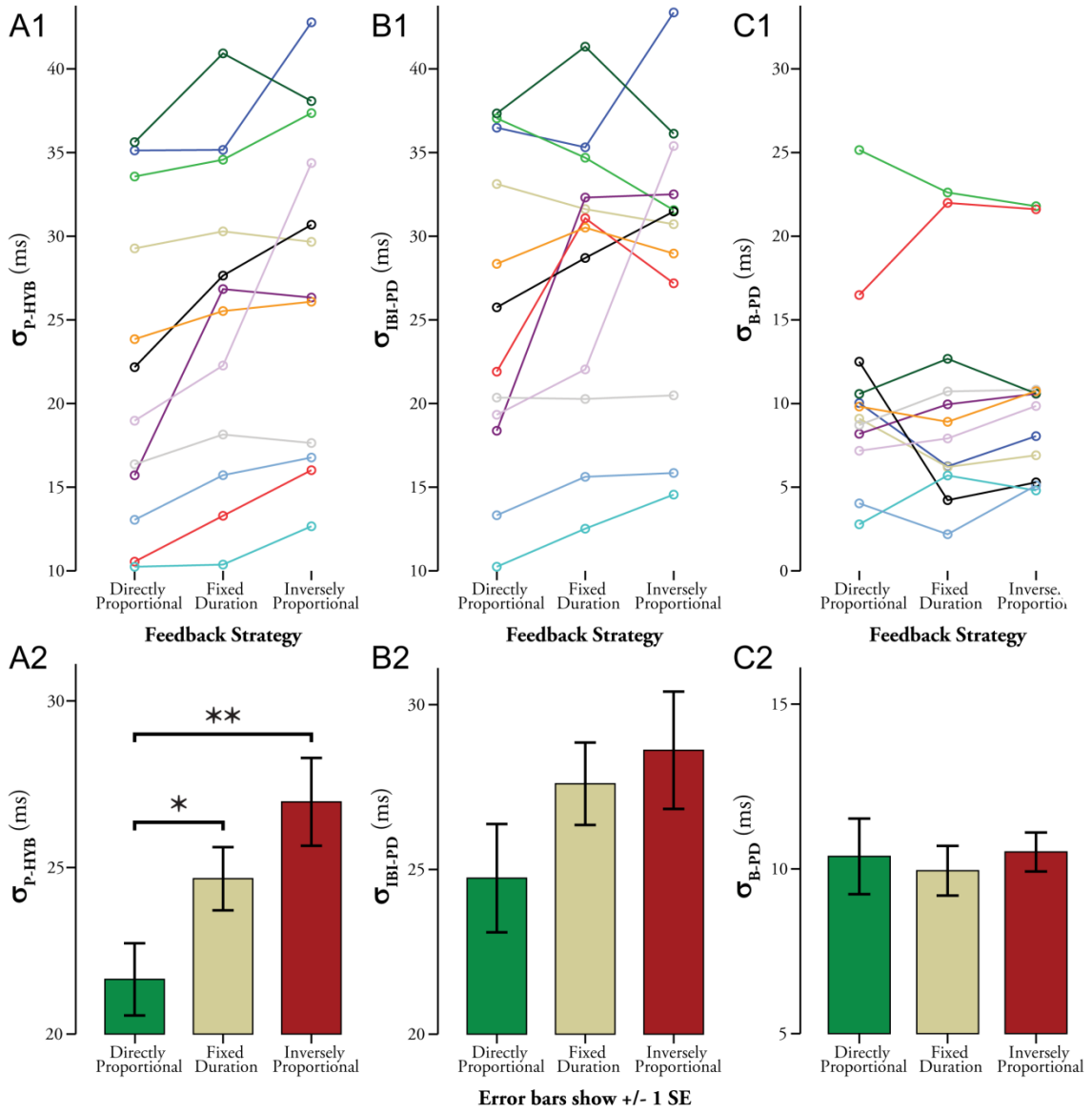

Figure 23. Statistical analysis of hybrid network variability observed in P_{HYB}, IBI_{PD}, and B_{PD}. Analysis by rANOVA and Bonferonni corrected pairwise comparisons reveal a statistically significant difference in standard deviation of P_{HYB} ($\sigma_{P\text{-}HYB}$) (A) due to VFU burst width strategy, with the directly proportional VFU burst width strategy having significantly less variability than both alternative strategies. Neither standard deviation of P_{HYB} ($\sigma_{IBI\text{-}PD}$) nor standard deviation of B_{PD} ($\sigma_{B\text{-}PD}$) exhibited statistically significant differences due to VFU burst width strategy. Error bars represent SE adjusted for repeated measures data.

DISCUSSION

In this study, using a combination of experimental and modeling methods, we have found a new means by which the pyloric network activity tends to maintain the phase of its activity intervals, and have presented evidence that suggests that this regulation may play a role in determining network activity period variability.

The cause of the pyloric network's tendency to exhibit strong cycle to cycle maintenance of LP burst duty cycle, and why some networks do not, remain open questions. A few features of the network may play a role in establishing this regulation. The presence of synaptic depression could give rise to a type of burst width regulation, while the relative absence of the same may bias synaptic feedback to be conserved in burst duration and not in burst duty cycle (Manor et al., 2003; Greenberg and Manor, 2005; Marder and Bucher, 2007; Mouser et al., 2008). Another possible contributing factor to differences seen in LP's burst duration regulation may arise from differences in levels of relative strength of the PY to LP synapse, where a strong synapse might terminate LP bursting effectively while a lack of strong feedback here may tend to defer termination of LP's burst to inhibition via AB/PD (Skinner et al., 1994).

The synapses in this system exhibit both graded and spike mediated inhibitory chemical components (Maynard, 1972; Maynard and Walton, 1975; Graubard, 1978; Graubard et al., 1980, 1983; Mulloney, 1987). In the intact network (Fig. 15C) these synapses allow AB/PD to impose intervals of strong inhibition on the LP and PY follower neurons while AB/PD is actively bursting, which ceases once AB/PD bursting terminates, which initiates post-inhibitory rebound in both LP and PY. But since there is

mutual inhibition between LP and PY and LP recovers from inhibition more quickly than PY (Marder and Calabrese 1996), active LP delays the onset of bursting in PY via the influence of the LP→PY synapse. This synaptic delay of PY onset not only helps determine the stereotyped triphasic bursting order observed in the pyloric network (Fig. 15), but may play a role in setting LP burst width due to synaptic feedback. LP and PY are finally inhibited by the next burst of AB/PD, which restarts the next cycle. With all of these complex synaptic interactions, LP burst width has the potential to be regulated by its synaptic interactions, but how exactly such regulation occurs in the pyloric network, and what its functional implications may be, are not well studied questions.

Finally, a recent study has shown that neuromodulation of crustacean gastric mill CPGs can counterbalance underlying perturbations to the circuit due to changes in temperature (Städele et al., 2015), which may indicate a role for mechanisms external to the network itself such as neuromodulation. That such neuromodulation may or may not be expected to operate on timescales coincident with the pyloric network's cycle period are not critical. A combination of relatively fast mechanisms may collectively create strong cycle-by-cycle regulation as an emergent property. Our results showing strong cycle-by-cycle regulation should in no way be taken as discounting the presence of slower mechanisms of phase maintenance. Statistical procedures such as the cross-correlation analysis employed here inherently have more limited ability to detect slower effects that occur over many cycles, especially in light of the limited statistical power common in electrophysiological studies. We can only conclude that there is strong correlation on a cycle-by-cycle basis between period and feedback burst duration in the pyloric networks we observed.

Why some of our networks did not show cycle-by-cycle phase maintenance, while there have been no reports to date of pyloric networks failing to exhibit phase maintenance as measured by imposing large changes in cycle period of a pyloric network, may at first seem contradictory, but testing for the presence of both cycle-by-cycle phase maintenance and phase maintenance due to imposed changes in pacemaker period in the same preparation was beyond the scope of our work. That the same processes may underlie both kinds of phase regulation is not clear, so it is unlikely that our findings cast any doubts on previous research on phase maintenance.

Our other major conclusion of this study was that a VFU designed to reproduce the cycle-by-cycle regulation of LP feedback burst width as closely as possible minimizes network variability of period. It does not necessarily impact variability of other intervals in the network, such as PD burst duration and interburst-interval. A superficial look at the results of Fig. 23 indicates that the primary interval being modulated to reduce variability would be the interburst-interval, but closer examination of the variability in each of these intervals in individual experiments (Fig. 23A1,B1,C1) indicates some unexpected relationships between variability of network period, PD burst duration, and PD interburst-interval that do not appear to be consistent from one animal to another. For example, in the green trace representing one experiment, while the directly proportional feedback strategy minimizes variability in period, it maximizes variability in both PD interburst-interval and burst duration, indicating a complex relationship that is not observed in other preparations.

Two of the VFU burst regulation strategies we used were based on observations in the biological pyloric network, while the third, inversely proportional, strategy was

chosen based upon mathematical symmetry and theoretical interest. But at least one computational study indicates that something like it could theoretically be possible, in the generation of anti-phase-maintaining bursts in a modified model based upon a pyloric neuron (Hooper et al., 2009).

Limitations

The presence of autocorrelation in some preparations made it difficult to conclude that any phase maintenance observed occurred primarily on a cycle-by-cycle basis, in contrast to preparations that exhibited no autocorrelation of network period. But the absence of more than one statistically significant peak in the cross-correlation in preparations that did not exhibit autocorrelation, combined with the lag 0 cross-correlation peaks being the largest significant peaks in the cross-correlation of preparations with autocorrelation, indicates a likely similarity.

In our hybrid networks we designed our VFU burst width regulation strategies to reproduce phase maintenance as it would occur in the pyloric network as closely as we can within the limits of causality, in not being able to calculate and deliver a phase maintained burst width based upon a measured network period that has yet to complete its cycle. As a result there was an offset of one cycle of burst width regulation relative to that observed in the biological networks. This distinction does not appear to be as consequential for neurons with significant autocorrelation in network period fluctuations due to the nature of fluctuations occurring on a timescale slower than one cycle period, which causes the feedback burst width control to perform very similarly to what would be expected in a biological network. The presence or absence of autocorrelation in network

period did not appear to be a factor in the directly proportional burst regulation strategy's tendency to most strongly minimize network period variability among the strategies we studied. Since the presence of autocorrelation as in Figs. 20,21 tends to make the hybrid network results more similar to what would occur in a network with no lag in cycle-by-cycle burst width regulation—such as a biological pyloric network—by reducing the importance of individual cycle burst width due to fluctuations that occur of many cycles, for these preparations we can conclude that the presence of autocorrelation helped overcome the limitations of our hybrid networks.

CHAPTER 5: CONCLUSIONS

The goal of much study in neuroscience is to one day understand how astonishingly complex neural networks give rise to the activity and wondrous, almost incomprehensible computation that undergirds life and is at once flexible, powerful, intricate, delicate, and mysterious. One intermediate goal along that path seeks to address the hope that we may one day be able to treat or even cure dysfunction of the nervous system that gives rise to debilitating disorders such as Parkinson's disease, schizophrenia, and epilepsy. Because such neural disorders are often marked by dysfunction in rhythmogenesis (Brown et al., 2001; Worrell et al., 2004; Uhlhaas et al., 2008; Zijlmans et al., 2012), understanding links between underlying neural network properties and their associated rhythmic activity may one day shed light on the origins of disease (Yu et al., 2008; Rieubland et al., 2014).

Our focus was on discovering dynamical response properties of networks capable of exerting control over the variability of rhythmic neuronal network activity, and found two such properties: phase response properties of a feedback neuron, and rapid phase regulation of burst width in a feedback neuron.

AIM 1: CHAPTER 2

We addressed how feedback to a bursting biological pacemaker with intrinsic variability in cycle length can affect that variability. Specifically we examined a hybrid circuit constructed of an isolated crab AB/PD pyloric pacemaker receiving virtual feedback via dynamic clamp. This virtual feedback generated artificial synaptic input to

PD with timing determined by adjustable phase response dynamics that mimic average burst intervals generated by LP in the intact pyloric network. Using this system we measured network period variability dependence on the feedback element's phase response dynamics, and find that a constant response interval confers minimum variability. We further found that these optimal dynamics are characteristic of the biological pyloric network.

AIM 2: CHAPTER 2

Building upon previous theoretical work mapping the firing intervals in one cycle onto the firing intervals in the next cycle, we created a theoretical map of the distribution of all firing intervals in one cycle to the distribution of firing intervals in the next cycle. We then obtained an integral equation for a stationary self-consistent distribution of the network periods of the hybrid circuit, which can be solved numerically given the uncoupled pacemaker's distribution of intrinsic periods, nature of the network's feedback, and phase resetting characteristics of the pacemaker. The stationary distributions obtained in this manner are strongly predictive of the experimentally observed distributions of hybrid network period. This theoretical framework can provide insight into optimal feedback schemes for minimizing variability to increase reliability or maximizing variability to increase flexibility in central pattern generators driven by pacemakers with feedback.

AIM 3: CHAPTER 3

In Chapter 3, we found a novel mechanism by which pyloric networks regulate their activity intervals: cycle-by-cycle changes in feedback burst width proportional to period. Using dynamic clamp, we further found evidence that this regulation may play a role in optimizing pyloric networks' activity variability by creating models that reproduced this regulation and some alternative regulation strategies, including no regulation (constant burst duration) and inversely proportional burst width regulation, and comparing the variability produced in response to interaction with identical biological AB/PD pacemakers . To date this indicates that out of the three overall properties for which the pyloric system has been examined for its effect on variability due to said underlying property, including inhibitory/excitatory makeup of its synapses (Selverston et al., 2000; Sieling et al., 2009), phase response properties of feedback neurons (Hooper et al., 2015), and burst width regulation of feedback neurons (Chapter 3), the pyloric network has proven to be optimal at minimizing network variability in every case.

IMPLICATIONS FOR FUTURE WORK

Our findings imply that for many kinds of computational studies, we may not be able to accurately assess the realism of constructed models if we neglect consideration of how real networks are adapted to variability. Classification of models based upon how they are adapted to realistic stochastic processes is not currently standard practice, and presents a number of challenges that must be overcome before such tests could be widely adopted in computational modeling. The nature of variability in each circuit of interest

must first be appropriately understood and modeled. Progress in this area is ongoing (Norman et al., 2013; Norman, 2014), but is not yet fully understood in most systems.

Due to the exploratory nature of this research, our studies were performed in small networks with identified neurons and known connections. In combination with our hybrid network techniques, this allowed us to study simple network interactions one at a time. Generalizing these findings to more complex networks is a critically important next step for understanding and modeling the circuits of the brain and vertebrate nervous system. Vertebrate neuronal networks are no less intensely studied using computational modeling than invertebrate neuronal networks such as those we studied here, and in fact many vertebrate modeling studies have already utilized activity variability to gain insight into neural function such as gain control and propagation of spike synchrony in cortical networks (Diesmann et al., 1999; Chance et al., 2002; Rothman et al., 2009; Moldakarimov et al., 2015). However, due to the scale and multi-layered hierarchical organization of cortical networks (Felleman and Van Essen, 1991), they may pose the greatest challenge to finding adaptive differences in network properties due to variability, particularly given their demonstrated low levels of spike time variability (Mainen and Sejnowski, 1995; Bair and Koch, 1996; Haider et al., 2010). Considering the advent of a new understanding of the vertebrate spinal circuits that generate locomotor patterns as arising from a distributed organization of distinct rhythmic modules (Hägglund et al., 2013; McLean and Dougherty, 2015)—together with their CPG action and amenability to new optogenetic tools—the spinal motor system is a well-positioned system in which to begin exploration of the relationships between network properties and stochastic network activity in vertebrate mammals.

REFERENCES

Archila S. Experimental and computational evidence for regulation of synaptic conductance via graded homeostasis of post-synaptic chloride concentration. PhD Thesis, Emory University, Atlanta, GA, 2013.

Archila S, **Prinz AA**. Investigating synaptic plasticity in the crab Cancer borealis pyloric circuit and in a computational pyloric model network database. *BMC Neurosci* 13: P69, 2012.

Bair W, **Koch C**. Temporal precision of spike trains in extrastriate cortex of the behaving macaque monkey. *Neural Comput* 8: 1185–1202, 1996.

Bal T, **Nagy F**, **Moulins M**. The pyloric central pattern generator in crustacea: a set of conditional neural oscillators. *J Comp Physiol A* 163: 715–727, 1988.

Bartos M, **Manor Y**, **Nadim F**, **Marder E**, **Nusbaum MP**. Coordination of Fast and Slow Rhythmic Neuronal Circuits. *J Neurosci* 19: 6650–6660, 1999.

Berger H. Über das Elektroenkephalogramm des Menschen. *Arch Psychiatr Nervenkr* 87: 527–70, 1929.

Bidaut M. Pharmacological dissection of pyloric network of the lobster stomatogastric ganglion using picrotoxin. *J Neurophysiol* 44: 1089–1101, 1980.

Brown P, **Oliviero A**, **Mazzone P**, **Insola A**, **Tonali P**, **Di Lazzaro V**. Dopamine dependency of oscillations between subthalamic nucleus and pallidum in Parkinson's Disease. *J Neurosci* 21: 1033–38, 2001.

Bucher D, **Prinz AA**, **Marder E**. Animal-to-Animal Variability in Motor Pattern Production in Adults and during Growth. *J Neurosci* 25: 1611–1619, 2005.

Bucher D, **Taylor AL**, **Marder E**. Central pattern generating neurons simultaneously express fast and slow rhythmic activities in the stomatogastric ganglion. *J Neurophysiol* 95: 3617–3632, 2006.

Buzsáki G. Neuronal oscillations in cortical networks. *Science* 304: 1926–9, 2004.

Buzsáki G, **Llinás R**, **Berthoz A**, **Christen Y**. *Temporal Coding in the Brain*. Berlin: Springer-Verlag, 1994.

Canavier CC. Pulse Coupled Oscillators. In: *Encyclopedia of Computational Neuroscience: SpringerReference*. New York: Springer, 2014, p. DOI 10.1007/978–1–4614–7320–6_774–1.

Chance FS, **Abbott LF**, **Reyes AD**. Gain modulation from background synaptic input. *Neuron* 35: 773–782, 2002.

Clemens S, **Combes D**, **Meyrand P**, **Simmers J**. Long-Term Expression of Two Interacting Motor Pattern-Generating Networks in the Stomatogastric System of Freely Behaving Lobster. *J Neurophysiol* 79: 1396–1408, 1998.

Cui J, **Canavier CC**, **Butera RJ**. Functional phase response curves: a method for understanding synchronization of adapting neurons. *J Neurophysiol* 102: 387–398, 2009.

Dando MR, **Chanussot B**, **Nagy F**. Activation of command fibres to the stomatogastric ganglion by input from a gastric mill proprioceptor in the crab, Cancer pagurus. *Mar Behav Physiol* 2: 197–228, 1973.

Daur N, **Bryan AS**, **Garcia VJ**, **Bucher D**. Short-Term Synaptic Plasticity Compensates for Variability in Number of Motor Neurons at a Neuromuscular Junction. *J Neurosci* 32: 16007–16017, 2012.

Deister CA, **Dodla R**, **Barraza D**, **Kita H**, **Wilson CJ**. Firing rate and pattern heterogeneity in the globus pallidus arise from a single neuronal population. *J Neurophysiol* 109: 497–506, 2013.

Dickinson PS. Interactions among neural networks for behavior. *Curr Opin Neurobiol* 5: 792–798, 1995.

Diesmann M, **Gewaltig M-O**, **Aertsen A**. Stable propagation of synchronous spiking in cortical neural networks. *Nature* 402: 529–533, 1999.

Dorval AD, **Christini DJ**, **White JA**. Real-Time linux dynamic clamp: a fast and flexible way to construct virtual ion channels in living cells. *Ann Biomed Eng* 29: 897–907, 2001.

Engel A, **Fries P**, **Singer W**. Dynamic predictions - oscillations and synchrony in top-down processing. *Nat Rev Neurosci* 2: 704–16, 2001.

Ermentrout B. Type I Membranes, Phase Resetting Curves, and Synchrony. *Neural Comput* 8: 979–1001, 1996.

Ermentrout GB, **Beverlin B**, **Troyer T**, **Netoff TI**. The variance of phase-resetting curves. *J Comput Neurosci* 31: 185–197, 2011.

Ermentrout GB, **Chow CC**. Modeling neural oscillations. *Physiol Behav* 77: 629–33, 2002.

Faisal AA, **Selen LPJ**, **Wolpert DM**. Noise in the nervous system. *Nat Rev Neurosci* 9: 292–303, 2008.

Faul F, **Erdfelder E**, **Lang A-G**, **Buchner A**. G*Power 3: a flexible statistical power analysis program for the social, behavioral, and biomedical sciences. *Behav Res Methods* 39: 175–191, 2007.

Felleman DJ, **Van Essen DC**. Distributed hierarchical processing in the primate cerebral cortex. *Cereb Cortex N Y N 1991* 1: 1–47, 1991.

Gabriel JP, **Büschges A**. Control of stepping velocity in a single insect leg during walking. *Philos Trans R Soc Lond Math Phys Eng Sci* 365: 251–271, 2007.

Glass L. Synchronization and rhythmic processes in physiology. *Nature* 410: 277–284, 2001.

Goaillard J-M, **Taylor AL**, **Schulz DJ**, **Marder E**. Functional consequences of animal-to-animal variation in circuit parameters. *Nat Neurosci* 12: 1424–1430, 2009.

Golowasch J, **Marder E**. Ionic currents of the lateral pyloric neuron of the stomatogastric ganglion of the crab. *J Neurophysiol* 67: 318–331, 1992.

Grashow R, **Brookings T**, **Marder E**. Compensation for Variable Intrinsic Neuronal Excitability by Circuit-Synaptic Interactions. *J Neurosci* 30: 9145–9156, 2010.

Graubard K. Synaptic transmission without action potentials: input and output properties of nonspiking presynaptic neurons. *J Neurophysiol* 41: 1014–1025, 1978.

Graubard K, **Raper JA**, **Hartline D**. Graded synaptic transmission between identified spiking neurons. *J Neurophysiol* 50: 508–520, 1983.

Graubard K, **Raper JA**, **Hartline DA**. Graded synaptic transmission between spiking neurons. *Proc Natl Acad Sci* 77: 3733–3735, 1980.

Greenberg I, **Manor Y**. Synaptic depression in conjunction with A-current channels promote phase constancy in a rhythmic network. *J Neurophysiol* 93: 656–677, 2005.

Gutierrez GJ, **Grashow RG**. Cancer borealis stomatogastric nervous system dissection. *J Vis Exp JoVE* , 2009.

Gutierrez GJ, **O'Leary T**, **Marder E**. Multiple Mechanisms Switch an Electrically Coupled, Synaptically Inhibited Neuron between Competing Rhythmic Oscillators. *Neuron* 77: 845–858, 2013.

Hägglund M, **Dougherty KJ**, **Borgius L**, **Itohara S**, **Iwasato T**, **Kiehn O**. Optogenetic dissection reveals multiple rhythmogenic modules underlying locomotion. *Proc Natl Acad Sci* 110: 11589–11594, 2013.

Haider B, **Krause MR**, **Duque A**, **Yu Y**, **Touryan J**, **Mazer JA**, **McCormick DA**. Synaptic and network mechanisms of sparse and reliable visual cortical activity during nonclassical receptive field stimulation. *Neuron* 65: 107–121, 2010.

Harris-Warrick RM. Dynamic Biological Networks: The Stomatogastric Nervous System. Cambridge, MA: MIT Press, 1992, p. xvii, 328.

Harris-Warrick RM, **Marder E**. Modulation of neural networks for behavior. *Annu Rev Neurosci* 14: 39–57, 1991.

Hooper RM, **Prinz AA**. Dynamic Clamp in Biomimetic and Biohybrid Living-Hardware Systems. In: *Biohybrid Systems: Nerves, Interfaces, and Machines*, edited by Jung R. Weinheim, Germany: Wiley-VCH, 2011, p. 82–83.

Hooper RM, **Tikidji-Hamburyan RA**, **Canavier CC**, **Prinz AA**. Feedback Control of Variability in the Cycle Period of a Central Pattern Generator. *J Neurophysiol* 114: 2741–2752, 2015.

Hooper SL. Phase maintenance in the pyloric pattern of the lobster (Panulirus interruptus) stomatogastric ganglion. *J Comput Neurosci* 4: 191–205, 1997a.

Hooper SL. The pyloric pattern of the lobster (Panulirus interruptus) stomatogastric ganglion comprises two phase-maintaining subsets. *J Comput Neurosci* 4: 207–219, 1997b.

Hooper SL. Variation Is the Spice of Life. Focus on "Cycle-to-Cycle Variability of Neuromuscular Activity in Aplysia Feeding Behavior." *J Neurophysiol* 92: 40–41, 2004.

Hooper SL, **Buchman E**, **Weaver AL**, **Thuma JB**, **Hobbs KH**. Slow Conductances Could Underlie Intrinsic Phase-Maintaining Properties of Isolated Lobster (Panulirus interruptus) Pyloric Neurons. *J Neurosci* 29: 1834–1845, 2009.

Hooper SL, **Guschlbauer C**, **Uckermann G von**, **Büschges A**. Natural Neural Output That Produces Highly Variable Locomotory Movements. *J Neurophysiol* 96: 2072–2088, 2006.

Horn CC, **Zhurov Y**, **Orekhova IV**, **Proekt A**, **Kupfermann I**, **Weiss KR**, **Brezina V**. Cycle-to-Cycle Variability of Neuromuscular Activity in Aplysia Feeding Behavior. *J Neurophysiol* 92: 157–180, 2004.

Hudson AE, **Prinz AA**. Conductance Ratios and Cellular Identity. *PLoS Comput Biol* 6: e1000838, 2010.

Izhikevich EM, **Desai NS**, **Walcott EC**, **Hoppensteadt FC**. Bursts as a unit of neural information: Selective communication via resonance. *Trends Neurosci* 26: 161–167, 2003.

Katz PS, **Sakurai A**, **Clemens S**, **Davis D**. Cycle period of a network oscillator is independent of membrane potential and spiking activity in individual central pattern generator neurons. *J Neurophysiol* 92: 1904–1917, 2004.

Koshiya N, **Smith JC**. Neuronal pacemaker for breathing visualized in vitro. *Nature* 400: 360–363, 1999.

Lamb DG, **Calabrese RL**. Small is beautiful: models of small neuronal networks. *Curr Opin Neurobiol* 22: 670–675, 2012.

Larson HJ, **Shubert BO**. *Probabilistic Models in Engineering Sciences, Volume I: Random Variables and Stochastic Processes*. New York: John Wiley & Sons, 1979.

Liu Z, **Golowasch J**, **Marder E**, **Abbott LF**. A Model Neuron with Activity-Dependent Conductances Regulated by Multiple Calcium Sensors. *J Neurosci* 18: 2309–2320, 1998.

Llinás R. The intrinsic electrophysiological properties of mammalian neurons: Insights into central nervous system function. *Science* 242: 1654–1664, 1988.

MacLean JN, **Zhang Y**, **Johnson BR**, **Harris-Warrick RM**. Activity-independent homeostasis in rhythmically active neurons. *Neuron* 37: 109–120, 2003.

Mainen ZF, **Sejnowski TJ**. Reliability of spike timing in neocortical neurons. *Science* 268: 1503–1506, 1995.

Mamiya A, **Nadim F**. Dynamic Interaction of Oscillatory Neurons Coupled with Reciprocally Inhibitory Synapses Acts to Stabilize the Rhythm Period. *J Neurosci* 24: 5140–5150, 2004.

Manor Y, **Bose A**, **Booth V**, **Nadim F**. Contribution of synaptic depression to phase maintenance in a model rhythmic network. *J Neurophysiol* 90: 3513–3528, 2003.

Maran SK, **Sieling FH**, **Demla K**, **Prinz AA**, **Canavier CC**. Responses of a bursting pacemaker to excitation reveal spatial segregation between bursting and spiking mechanisms. *J Comput Neurosci* 31: 419–440, 2011.

Marder E, **Bucher D**. Central pattern generators and the control of rhythmic movements. *Curr Biol* 11: R986–R996, 2001.

Marder E, **Bucher D**. Understanding circuit dynamics using the stomatogastric nervous system of lobsters and crabs. *Annu Rev Physiol* 69: 291–316, 2007.

Maxwell SE. Pairwise Multiple Comparisons in Repeated Measures Designs. *J Educ Behav Stat* 5: 269–287, 1980.

Maynard DM. Simpler Networks. *Ann N Y Acad Sci* 193: 59–72, 1972.

Maynard DM, **Walton KD**. Effects of maintained depolarization of presynaptic neurons on inhibitory transmission in lobster neuropil. *J Comp Physiol* 97: 215–243, 1975.

McLean DL, **Dougherty KJ**. Peeling back the layers of locomotor control in the spinal cord. *Curr Opin Neurobiol* 33: 63–70, 2015.

Miller JP, **Selverston AI**. Rapid killing of single neurons by irradiation of intracellularly injected dye. *Science* 206: 702–704, 1979.

Miller JP, **Selverston AI**. Mechanisms underlying pattern generation in lobster stomatogastric ganglion as determined by selective inactivation of identified neurons. 2. Oscillatory properties of pyloric neurons. *J Neurophysiol* 48: 1378–1391, 1982.

Moldakarimov S, **Bazhenov M**, **Sejnowski TJ**. Feedback stabilizes propagation of synchronous spiking in cortical neural networks. *Proc Natl Acad Sci* 112: 2545–2550, 2015.

Morris LG, **Hooper SL**. Muscle response to changing neuronal input in the lobster (Panulirus interruptus) stomatogastric system: Spike number- versus spike frequency-dependent domains. *J Neurosci* 17: 5956–5971, 1997.

Mouser C, **Nadim F**, **Bose A**. Maintaining phase of the crustacean tri-phasic pyloric rhythm. *J Math Biol* 57: 161–181, 2008.

Mulloney B. Organization of the stomatogastric ganglion of the spiny lobster. *J Comp Physiol* 122: 227–240, 1977.

Mulloney B. Neural circuits. In: *The Crustacean Stomatogastric System*, edited by Selverston AI, Moulins M. Berlin: Springer-Verlag, 1987, p. 57–77.

Nadim F, **Zhao S**, **Zhou L**, **Bose A**. Inhibitory feedback promotes stability in an oscillatory network. *J Neural Eng* 8: 065001, 2011.

Netoff TI, **Banks MI**, **Dorval AD**, **Acker CD**, **Haas JS**, **Kopell N**, **White JA**. Synchronization in Hybrid Neuronal Networks of the Hippocampal Formation. *J Neurophysiol* 93: 1197–1208, 2005.

Norman SE. Quantifying Dynamics and Variability in Neural Systems. PhD Thesis, Georgia Institute of Technology, Atlanta, GA, 2014.

Norman SE, **Canavier CC**, **Butera RJ**. Period drift in spiking neurons has a history component. Society for Neuroscience Annual Meeting. San Diego, CA: 2013.

O'Brien F, **Cousineau D**. Representing Error bars in within-subject designs in typical software packages. *Quant Methods Psychol* 10: 56–67, 2014.

Oprisan SA, **Canavier CC**. Stability Analysis of Rings of Pulse-Coupled Oscillators: The Effect of Phase Resetting in the Second Cycle After the Pulse Is Important at Synchrony and For Long Pulses. *Differ Equ Dyn Syst* 9: 243–258, 2001.

Oprisan SA, **Prinz AA**, **Canavier CC**. Phase resetting and phase locking in hybrid circuits of one model and one biological neuron. *Biophys J* 87: 2283–2298, 2004.

Press WH, **Teukolsky SA**, **Vetterling WT**, **Flannery BP**. *Numerical Recipes 3rd Edition: The Art of Scientific Computing*. 3rd Ed. Cambridge, UK ; New York: Cambridge University Press, 2007.

Preyer AJ, **Butera RJ**. Causes of transient instabilities in the dynamic clamp. *IEEE Trans Neural Syst Rehabil Eng* 17: 190–8, 2009.

Prinz AA, **Abbott LF**, **Marder E**. The dynamic clamp comes of age. *Trends Neurosci* 27: 218–224, 2004a.

Prinz AA, **Billimoria CP**, **Marder E**. Alternative to Hand-Tuning Conductance-Based Models: Construction and Analysis of Databases of Model Neurons. *J Neurophysiol* 90: 3998–4015, 2003a.

Prinz AA, **Bucher D**, **Marder E**. Similar network activity from disparate circuit parameters. *Nat Neurosci* 7: 1345–1352, 2004b.

Prinz AA, **Thirumalai V**, **Marder E**. The Functional Consequences of Changes in the Strength and Duration of Synaptic Inputs to Oscillatory Neurons. *J Neurosci* 23: 943–954, 2003b.

Ramirez J-M, **Tryba AK**, **Peña F**. Pacemaker neurons and neuronal networks: an integrative view. *Curr Opin Neurobiol* 14: 665–674, 2004.

Reinsch CH. Smoothing by spline functions. *Numer Math* 10: 177–183, 1967.

Rieubland S, **Roth A**, **Häusser M**. Structured connectivity in cerebellar inhibitory networks. *Neuron* 81: 913–29, 2014.

Rothman JS, **Cathala L**, **Steuber V**, **Silver RA**. Synaptic depression enables neuronal gain control. *Nature* 457: 1015–1018, 2009.

Russell D, **Hartline D**. Bursting neuronal networks: a reexamination. *Science* 200: 453–456, 1978.

Schultheiss NW, **Prinz AA**, **Butera RJ**, editors. Phase Response Curves in Neuroscience [Online]. Springer New York. http://link.springer.com/10.1007/978-1-4614-0739-3 [8 Oct. 2015].

Schulz DJ, **Goaillard J-M**, **Marder E**. Variable channel expression in identified single and electrically coupled neurons in different animals. *Nat Neurosci* 9: 356–362, 2006.

Schulz DJ, **Goaillard J-M**, **Marder EE**. Quantitative expression profiling of identified neurons reveals cell-specific constraints on highly variable levels of gene expression. *Proc Natl Acad Sci* 104: 13187–13191, 2007.

Selverston A. Invertebrate central pattern generator circuits. *Philos Trans R Soc Lond B Biol Sci* 365: 2329–45, 2010.

Selverston AI, **Moulins M**. The stomatogastric nervous system: Structure and function of a small neural network. *Prog Neurobiol* 7: 215–290, 1976.

Selverston AI, **Moulins M**. *The Stomatogastric Stomatogastric System*. Berlin: Springer-Verlag, 1987.

Selverston AI, **Rabinovich MI**, **Abarbanel HDI**, **Elson R**, **Szucs A**, **Pinto RD**, **Huerta R**, **Varona P**. Reliable circuits from irregular neurons: A dynamical approach to understanding central pattern generators. *J Physiol-Paris* 94: 357–374, 2000.

Sieling F, **Bédécarrats A**, **Simmers J**, **Prinz AA**, **Nargeot R**. Differential Roles of Nonsynaptic and Synaptic Plasticity in Operant Reward Learning-Induced Compulsive Behavior. *Curr Biol* 24: 941–950, 2014.

Sieling FH, **Archila SA**, **Hooper RM**, **Canavier CC**. Phase response theory extended to nonoscillatory network components. *Phys Rev E* 85, 2012.

Sieling FH, **Canavier CC**, **Prinz AA**. Predictions of phase-locking in excitatory hybrid networks: excitation does not promote phase-locking in pattern-generating networks as reliably as inhibition. *J Neurophysiol* 102: 69–84, 2009.

Skinner FK, **Kopell N**, **Marder E**. Mechanisms for oscillation and frequency control in reciprocally inhibitory model neural networks. *J Comput Neurosci* 1: 69–87, 1994.

Sokal RR, **Rohlf FJ**. *Biometry*. Macmillan, 1995.

Soofi W, **Archila S**, **Prinz AA**. Co-variation of ionic conductances supports phase maintenance in stomatogastric neurons. *J Comput Neurosci* 33: 77–95, 2012.

Soofi W, **Goeritz ML**, **Kispersky TJ**, **Prinz AA**, **Marder E**, **Stein W**. Phase maintenance in a rhythmic motor pattern during temperature changes in vivo. *J Neurophysiol* 111: 2603–2613, 2014.

Soofi W, **Prinz AA**. Differential effects of conductances on the phase resetting curve of a bursting neuronal oscillator. *J Comput Neurosci* 38: 539–558, 2015.

Spencer K, **Nestor P**, **Niznikiewicz M**, **Salisbury D**, **Shenton M**, **McCarley R**. Abnormal neural synchrony in schizophrenia. *J Neurosci* 23: 7407–11, 2003.

Städele C, **Heigele S**, **Stein W**. Neuromodulation to the Rescue: Compensation of Temperature-Induced Breakdown of Rhythmic Motor Patterns via Extrinsic Neuromodulatory Input. *PLoS Biol* 13: e1002265, 2015.

Stigen T, **Danzl P**, **Moehlis J**, **Netoff T**. Controlling spike timing and synchrony in oscillatory neurons. *J Neurophysiol* 105: 2074–2082, 2011.

Tang LS, **Goeritz ML**, **Caplan JS**, **Taylor AL**, **Fisek M**, **Marder E**. Precise Temperature Compensation of Phase in a Rhythmic Motor Pattern. *PLoS Biol* 8: e1000469, 2010.

Taylor AL, **Goaillard J-M**, **Marder E**. How multiple conductances determine electrophysiological properties in a multicompartment model. *J Neurosci* 29: 5573–5586, 2009.

Thirumalai V. Implications of cotransmission and neuromodulation for neural network function. PhD Thesis, Brandeis University, Waltham, MA, 2002.

Thounaojam US, **Cui J**, **Norman SE**, **Butera RJ**, **Canavier CC**. Slow noise in the period of a biological oscillator underlies gradual trends and abrupt transitions in phasic relationships in hybrid neural networks. *PLoS Comput Biol* 10: e1003622, 2014.

Thuma JB, **Hooper SL**. Quantification of Gastric Mill Network Effects on a Movement Related Parameter of Pyloric Network Output in the Lobster. *J Neurophysiol* 87: 2372–2384, 2002.

Tikidji-Hamburyan R, **Lin EC**, **Gasparini S**, **Canavier CC**. Effect of Heterogeneity and Noise on Cross Frequency Phase-Phase and Phase-Amplitude Coupling. *Netw-Comput Neural Syst* 25: 38–62, 2014.

Turrigiano G, **LeMasson G**, **Marder E**. Selective regulation of current densities underlies spontaneous changes in the activity of cultured neurons. *J Neurosci* 15: 3640–3652, 1995.

Uhlhaas P, **Haenschel C**, **Nikolić D**, **Singer W**. The role of oscillations and synchrony in cortical networks and their putative relevance for the pathophysiology of schizophrenia. *Schizophr Bull* 34: 927–43, 2008.

Weaver AL, **Hooper SL**. Follower Neurons in Lobster (Panulirus interruptus) Pyloric Network Regulate Pacemaker Period in Complementary Ways. *J Neurophysiol* 89: 1327–1338, 2003.

Wilson CJ. Active decorrelation in the basal ganglia. *Neuroscience* 250: 467–482, 2013.

Winfree AT. *The geometry of biological time*. 2nd ed. New York: Springer, 2001.

Worrell G, **Parish L**, **Cranstoun S**, **Jonas R**, **Baltuch G**, **Litt B**. High-frequency oscillations and seizure generation in neocortical epilepsy. *Brain* 127: 1496–1506, 2004.

Yu S, **Huang D**, **Singer W**, **Nikolić D**. A small world of neuronal synchrony. *Cereb Cortex* 18: 2891–901, 2008.

Zhao S, **Golowasch J**. Ionic Current Correlations Underlie the Global Tuning of Large Numbers of Neuronal Activity Attributes. *J Neurosci* 32: 13380–13388, 2012.

Zijlmans M, **Jiruska P**, **Zelmann R**, **Leijten F**, **Jefferys J**, **Gotman J**. High-frequency oscillations as a new biomarker in epilepsy. *Ann Neurol* 71: 169–78, 2012.